Contents

Lecture I – 1h

Boundary Layer and clouds

Marie Lothon
Laboratoire d'Aérologie, Toulouse

Photo by M. Scherrer

Diurnal cycle of the surface and low troposphere
Definition of the planetary boundary layer (PBL)

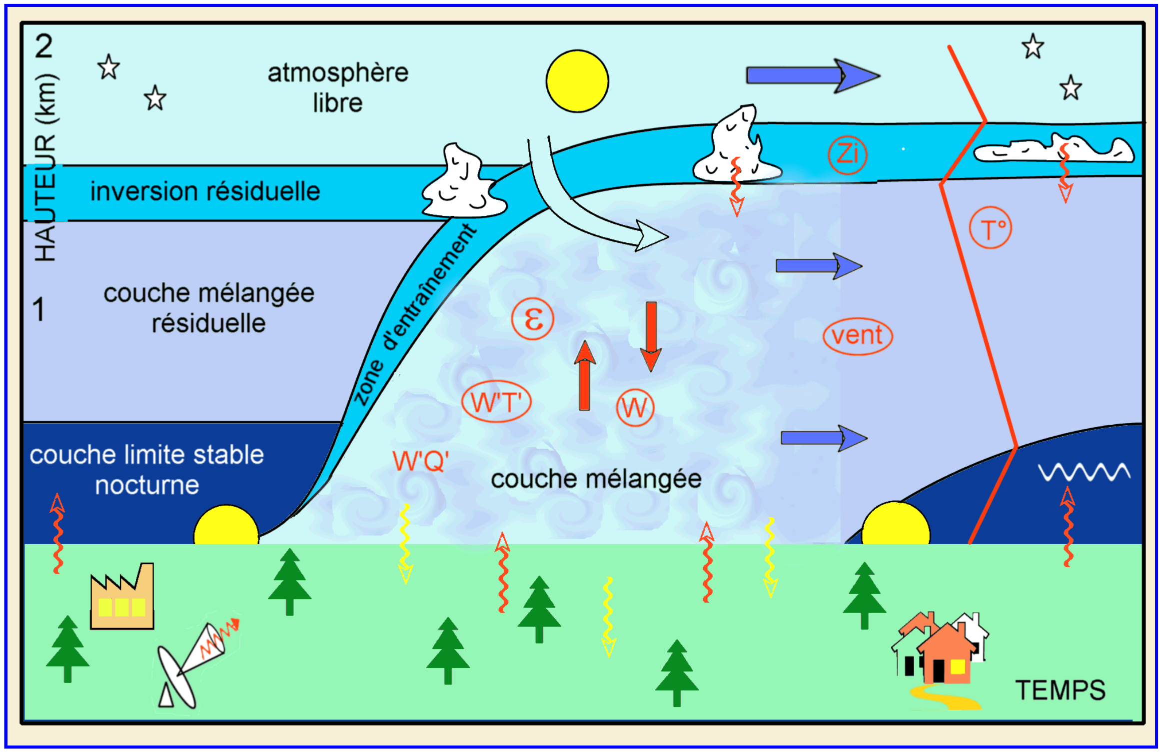

Courtesy of B. Campistron

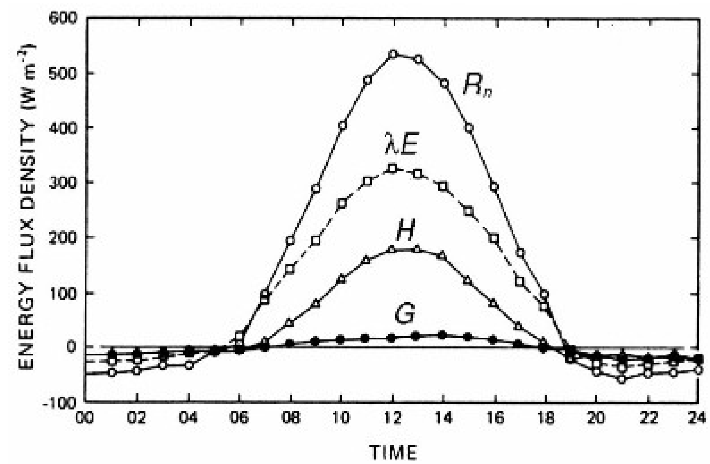

Figure 3. Diurnal cycle of the components of the surface energy budget in in cloudless conditions at a rural midlatitude site.

Courtesy of R. Hogan

Surface forcing

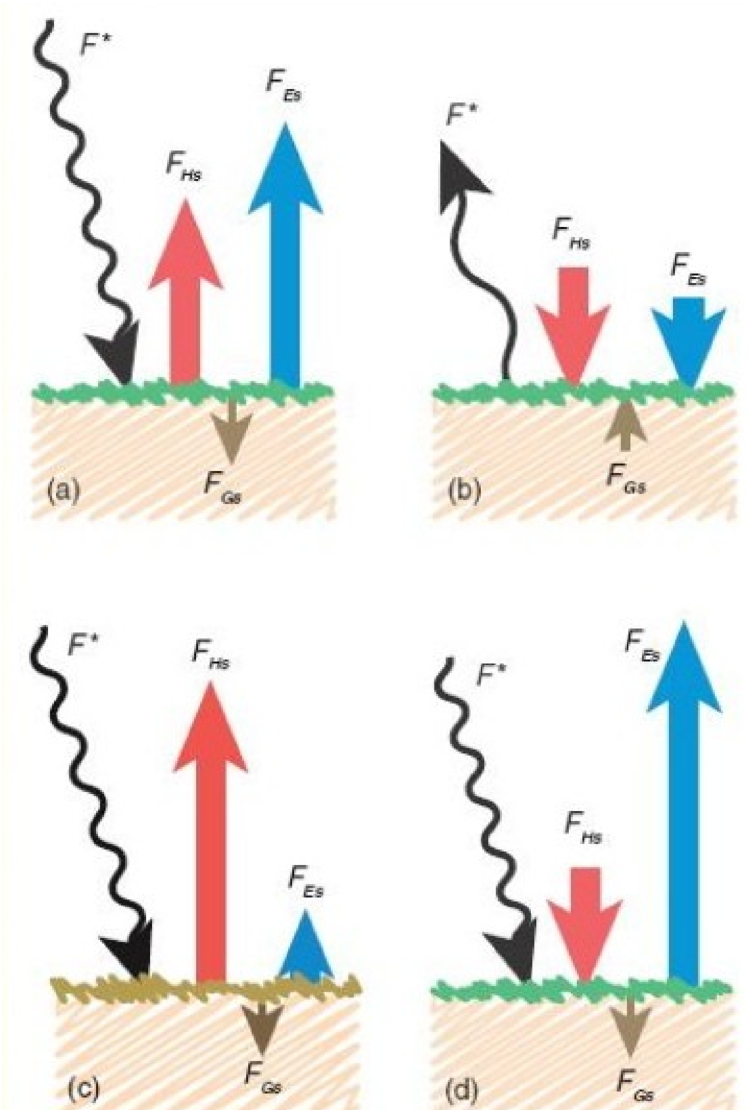

Wallace and Hobbes, 2006

(a) Daytime over moist surface
(b) Nighttime over moist surface
(c) Daytime over dry surface (Desert)
(d) Dry air over moist surface (Oasis)

Two important ways to consider the PBL and clouds:

(1) Vertical structure / Evolution
(2) Spatial variability / Scales

Photo by M. Scherrer

PBL vertical structure

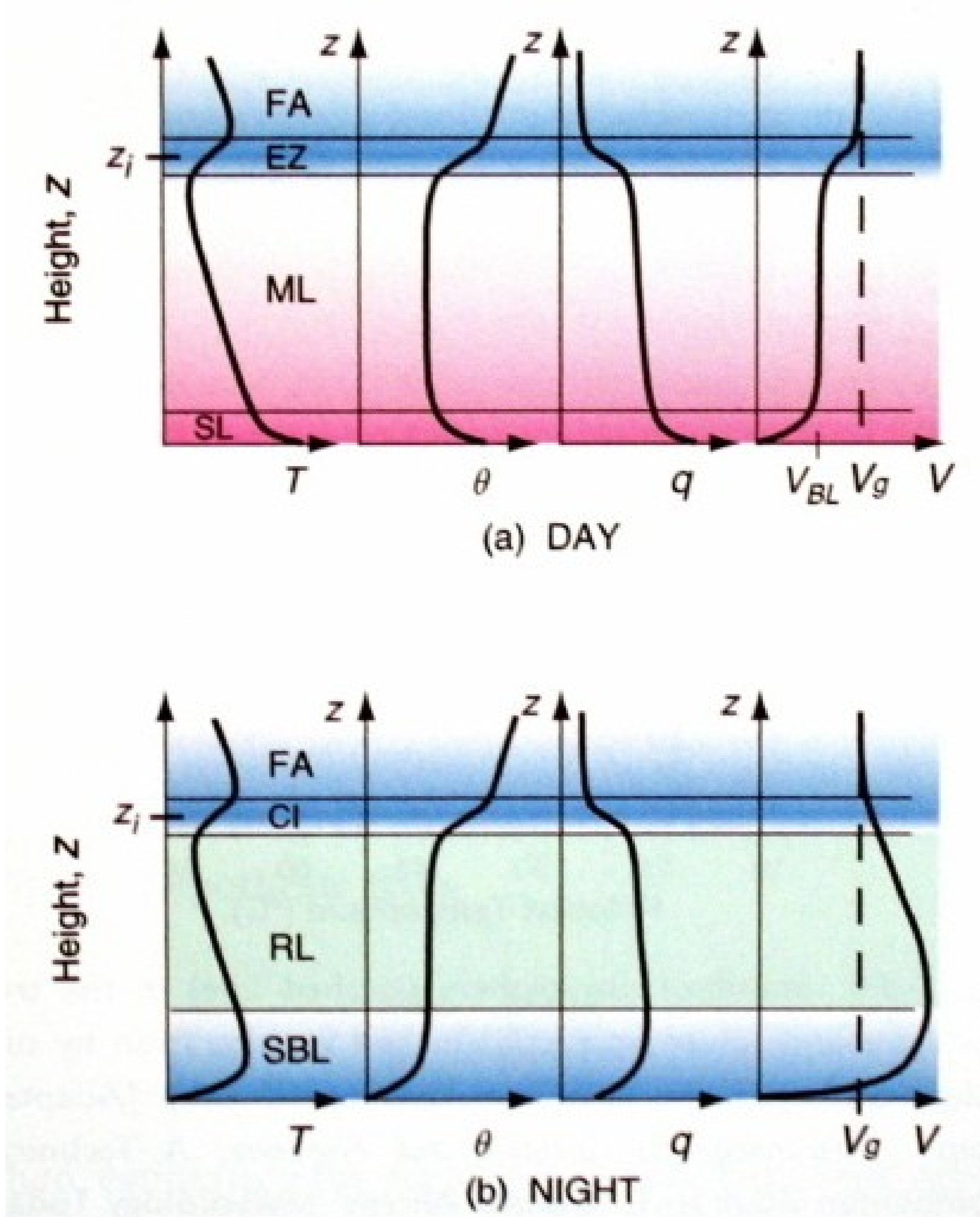

Stull, 1988
Wallace and Hobbes, 2006

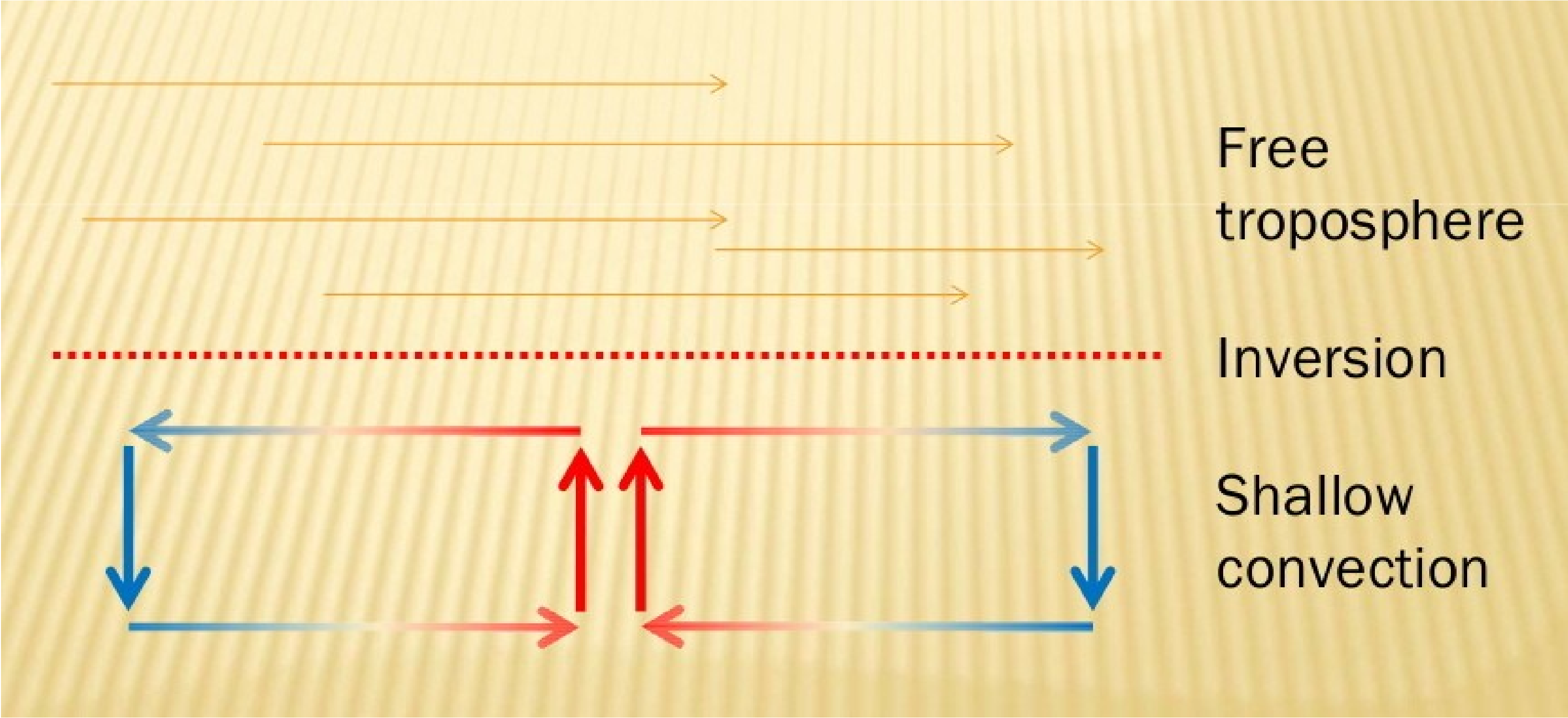

Courtesy of Colbert et al, 2008


Photo by G. Berry


Photo by G. Berry

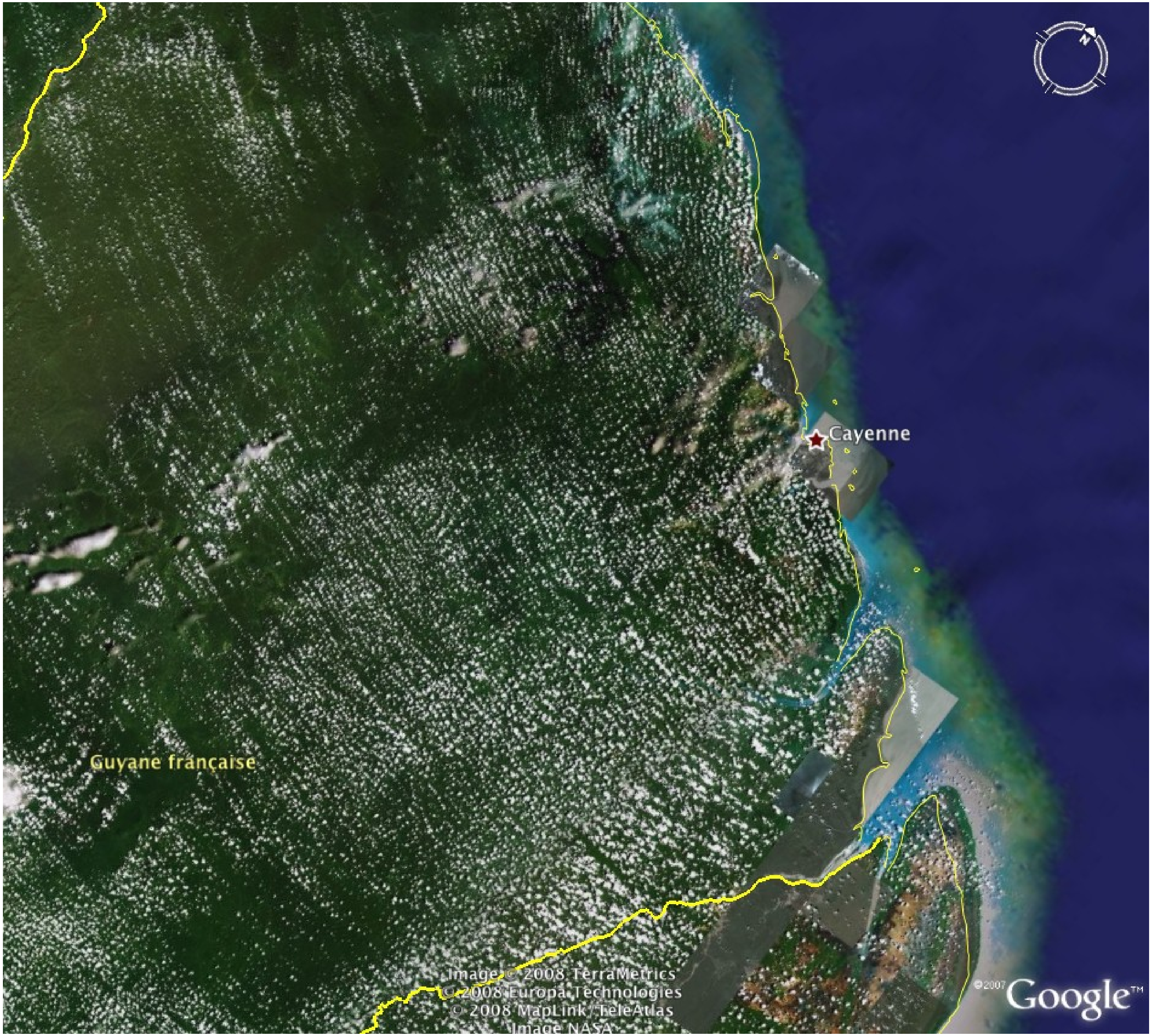
Cayenne
Guyane française
Image © 2008 TerraMetrics
© 2008 Europa Technologies
© 2008 MapLink / TeleAtlas
Image NASA
©2007 Google™

Rolls

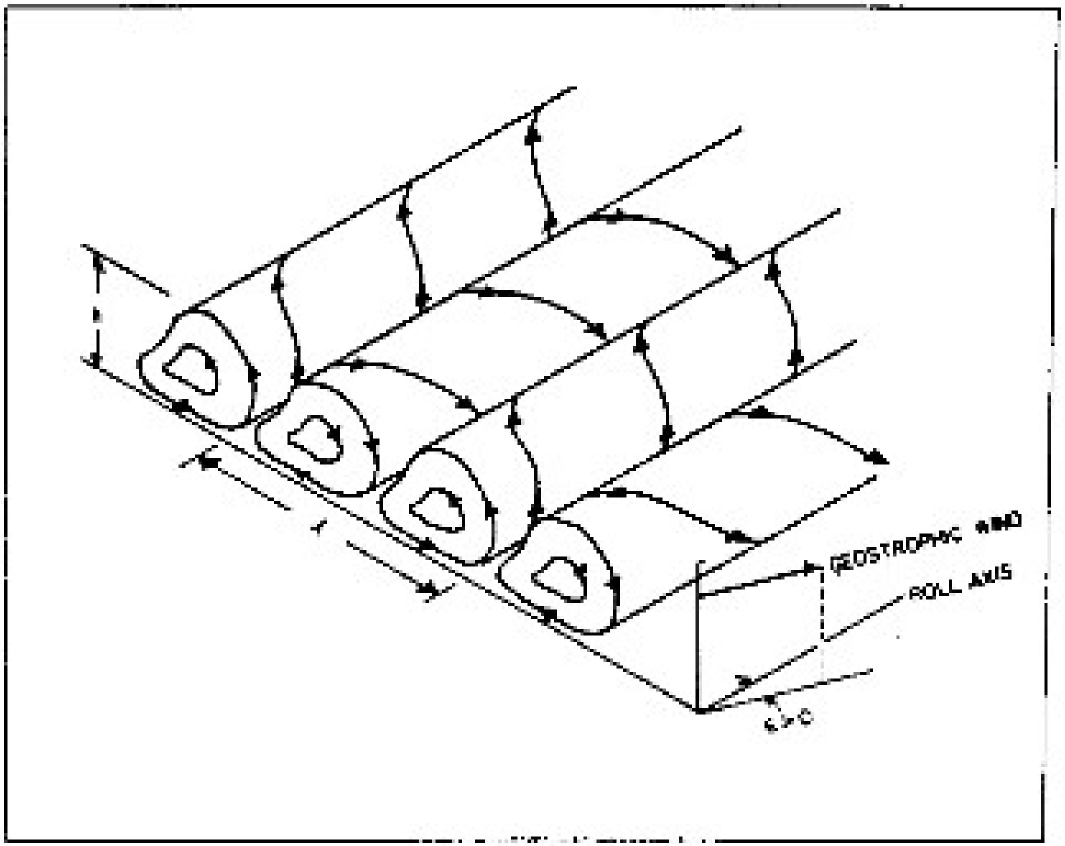

FIG. 1. Schematic diagram of horizontal convective rolls (Brown 1980; Kelly 1982).

See also Lemone, 1973
and Weckwerth et al, 1997

Reference	Approach	Cond. & loc.—No. of cases	TI	DI	$0 < -z_i/L < 21$ (Grossman 1982)	Wind > 5 m s^{-1} (Christian 1987)	Shear > 10^{-3}–10^{-2} s^{-1} (Miura 1986)	sh grad > 10^{-5} m^{-1} s^{-1} (Kuettner 1971)
Asai (1970a,b)	Theory	—	Y	Y	—	—	—	—
Atlas et al. (1986)	Lidar, Ac	CAO cstl—1	Y	IPI	—	Y	Y	—
Berger & Doviak (1979)	Radar	ClA OK—1	—	—	Y	Y	—	—
Brown (1980)	Theory	—	Y	IPI	—	—	—	—
Brümmer (1985)	Ac	ClA ocn—3	Y	IPI	Y	Y	—	—
Christian & Wakimoto (1989)	Radar, Pho, Sfc st, Sndg	ClA CO—1	—	—	N; 272	Y	Y	Y
Deardorff (1972)	3D model	—	Y	N	Y	—	—	—
Doviak and Berger (1980)	DDR, Tow	ClA OK—1	Y	IPI	—	Y	—	—
Faller (1965)	Lab	—	Y	—	—	Y	—	—
Ferrare et al. (1991)	Lidar	ClA OK—1	—	Y	N; 250	N; <2 m s^{-1}	—	—
Grossman (1982)	Ac	ClA ocn—4	Y	—	Y	—	—	—
Hildebrand (1980)	DDR	OK—1	—	Y	—	Y	—	—
Kelly (1984)	Radar, Ac	CAO L. MI—3	Y	Y	—	Y	—	—
Kristovich (1993)	Radar, Ac	LE L. MI—4	Y	Y	N; >136	Y	Y	Y; below $0.2z_i$
Kuettner (1971)	Pho, Theory	ClA—5	Y	Y	—	Y	Y	Y
LeMone (1973)	Ac, Tow	ClA—8	Y	IPI	Y	Y	—	—
Lilly (1966)	Theory	—	N	PI	—	Y	—	—
Mason & Sykes (1982)	2D model	—	—	N	Y	Y	—	—
Melfi et al. (1985)	Lidar	CAO ocn—1	—	—	Y	Y	—	—
Miura (1986)	Sat, Sndg	CAO ocn—61	Y	IPI	Y	Y	Y	N
Moeng & Sullivan (1994)	LES model	—	Y	Y	Y	Y	Y	N
Rabin et al. (1982)	DDR, Tow	ClA OK—1	—	—	Y	Y	—	—
Reinking et al. (1981)	DDR, Ac	ClA OK—1	—	—	Y	Y	—	—
Shirer (1986)	3D model	—	Y	PI	Y	—	—	—
Sykes & Henn (1989)	LES model	—	Y	Y	Y	—	Y	—
Walter & Overland (1984)	Sat, Ac	COA ocn—1	Y	IPI	Y	Y	Y	—
Current study	Radar, Sat, Sndg, Pho, Sfc st, Ac 3D model	ClA FL—100	Y	Y	Y	Y	N	N

Weckwerth et al, 1997

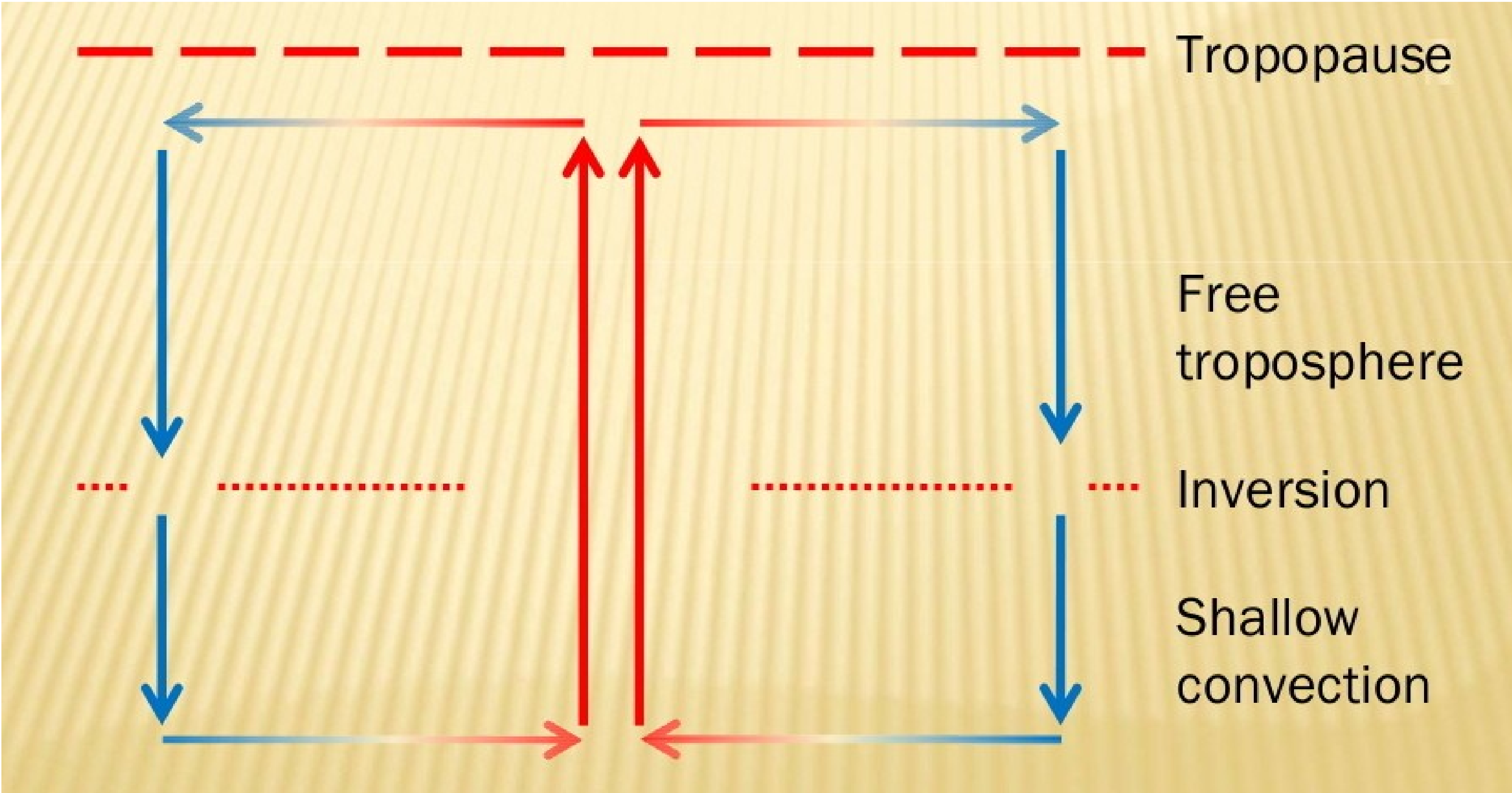

Courtesy of Colbert et al, 2008

Photo by M.
Lothon


Photo by M.


Photo by M.


Photo by M.

Atmospheric moist convection

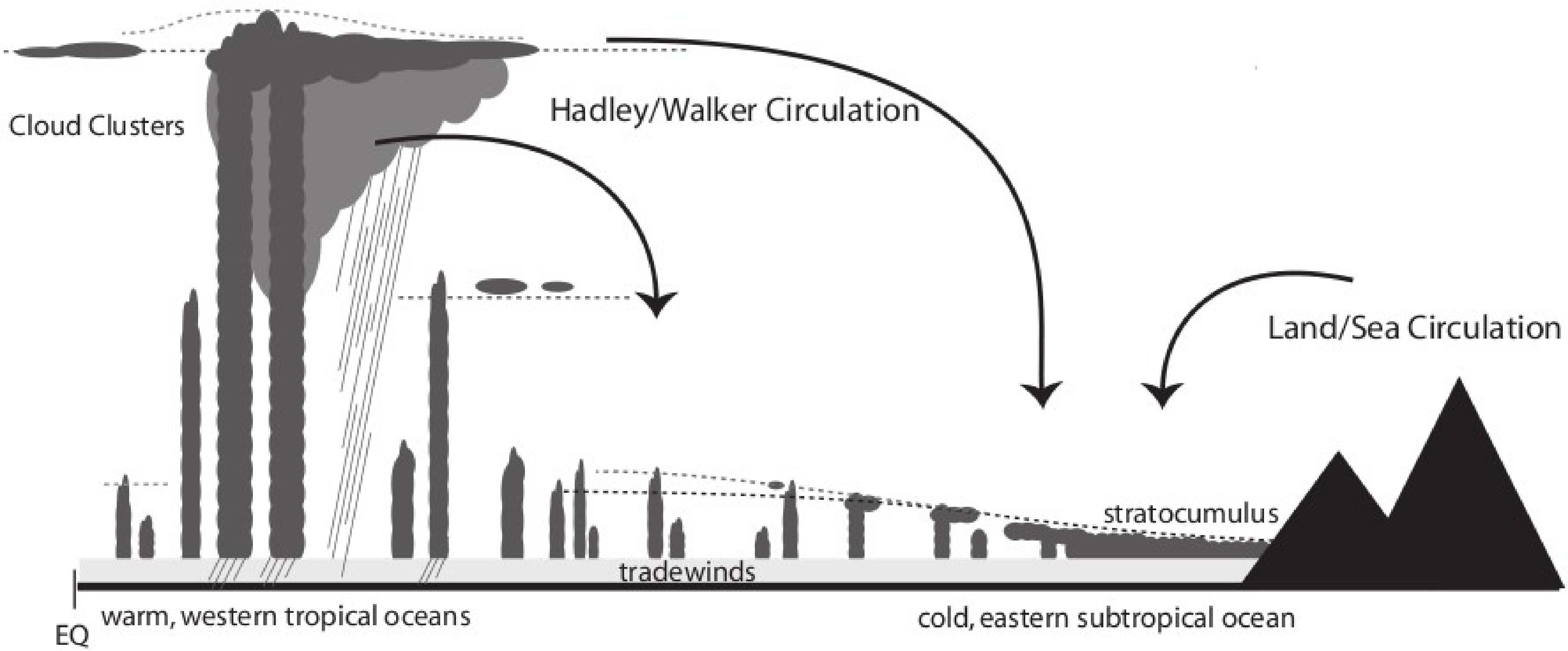

Stevens, 2005

Marine Stratocumulus

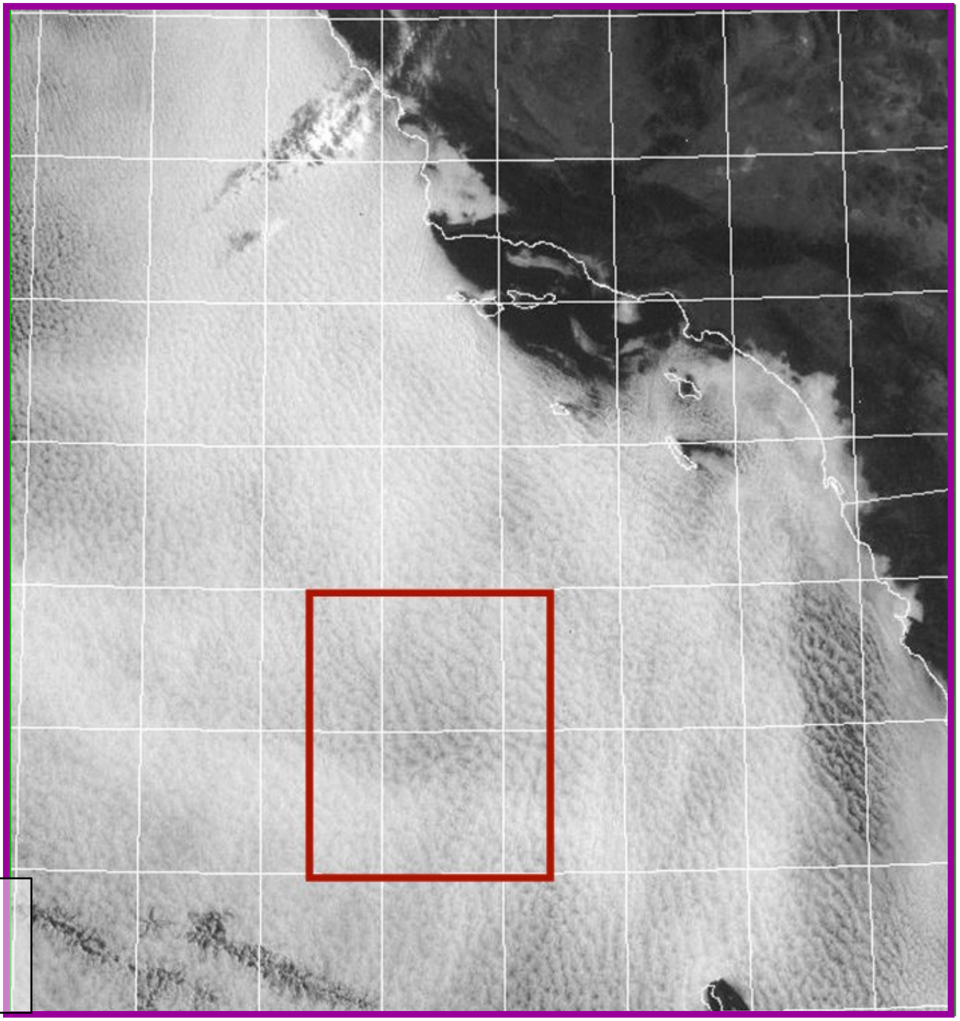

GOES Channel 1

July 24 2001 – 1200 UTC – DYCOMS RF07


Photo by G. Vali

Main processes
in the stratocumulus-topped marine boundary layer (STBL)

- **SW radiation**
- **Turbulent mixing**
- **Entrainment**
- **Cloud microphysics**

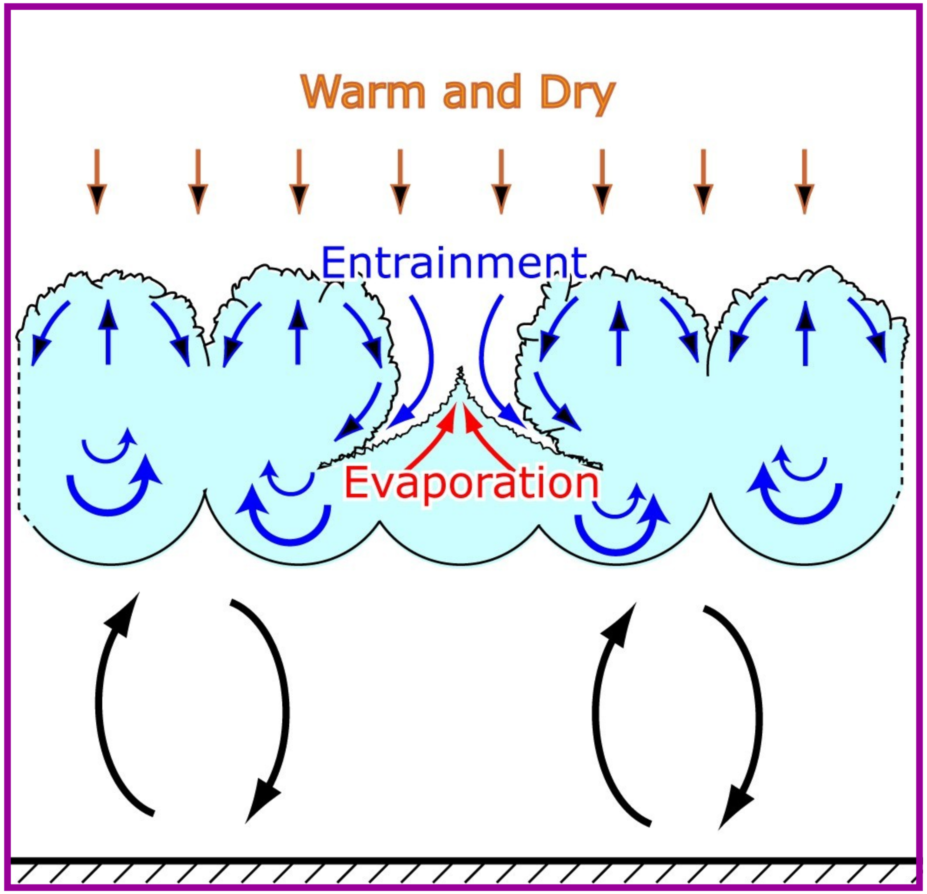

Conceptual diagram for the stratocumulus-topped PBL

Stevens, 2007

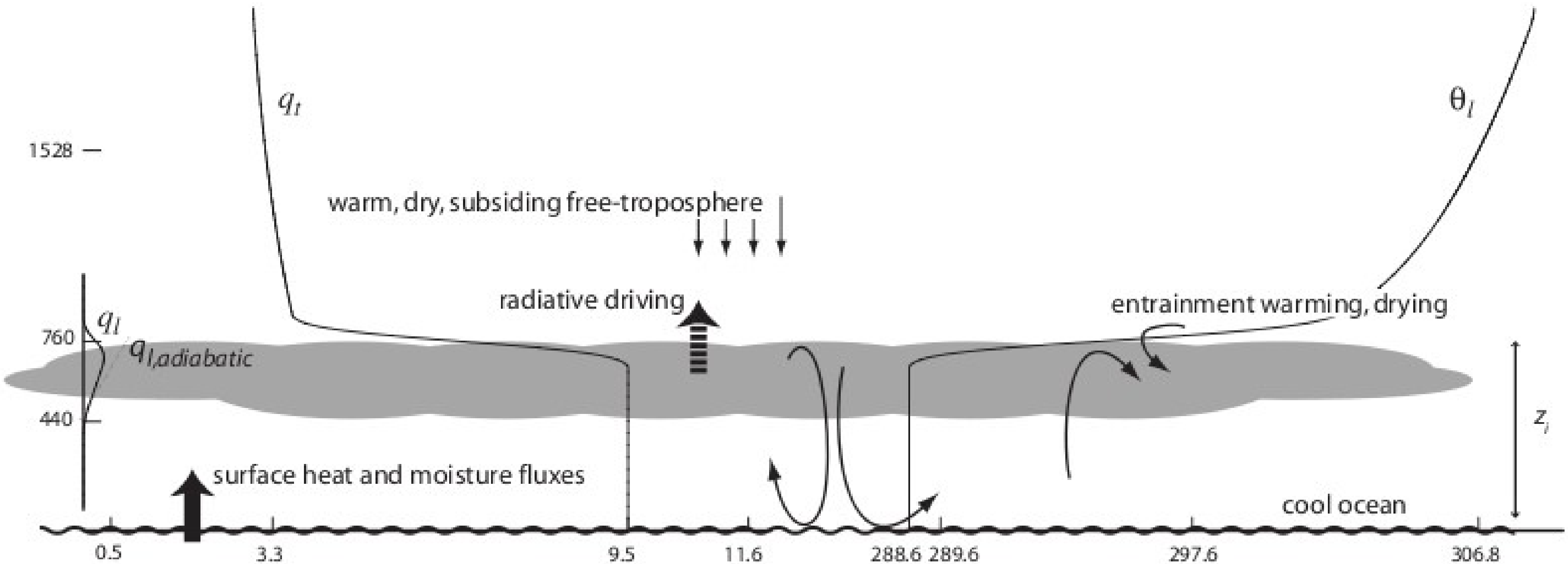

Stevens, 2007

VERTICAL STRUCTURE OF THE STBL

RF07
July 24

4 profiles made within a 4-hour period

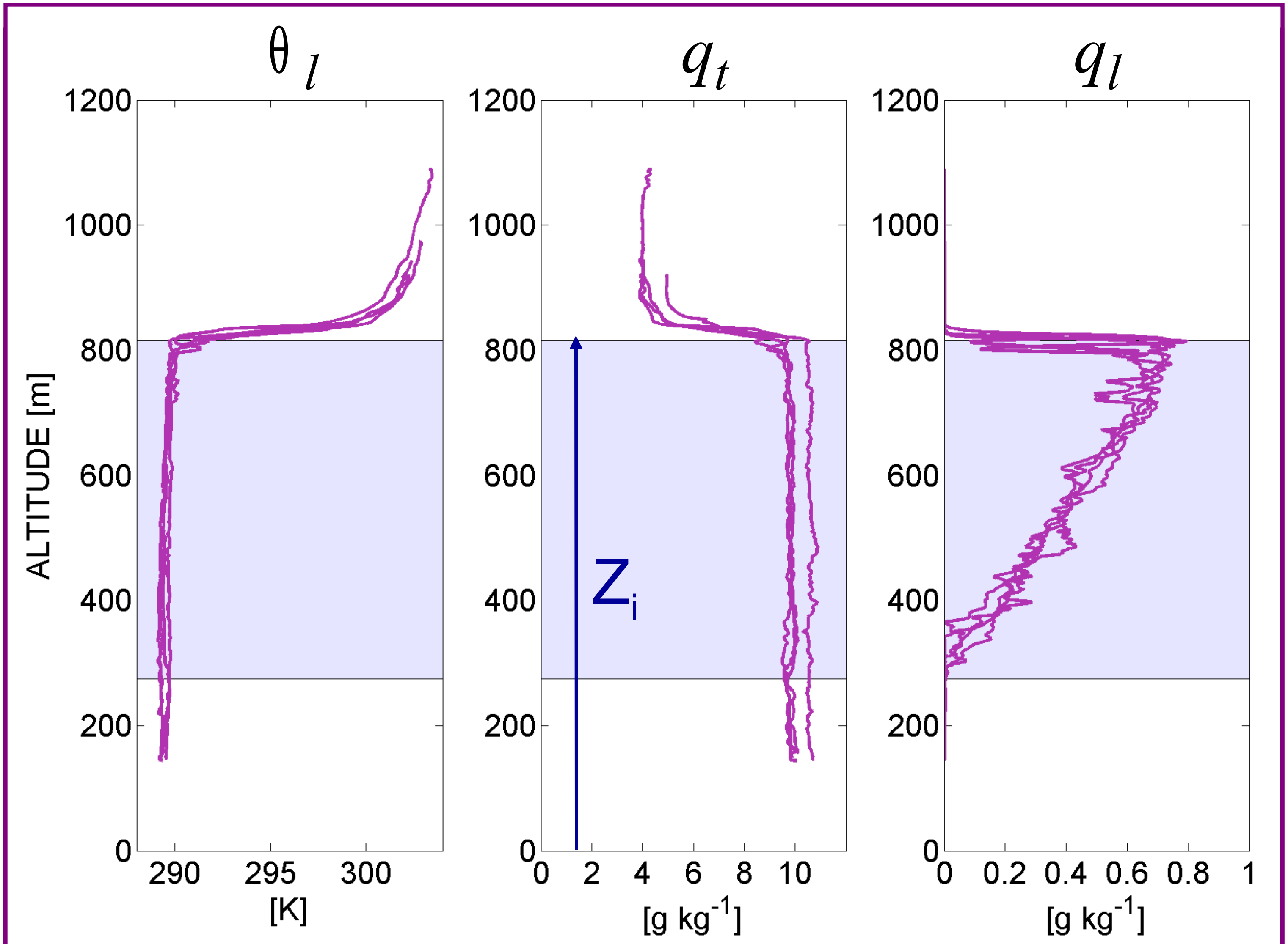

Pockets and Open cells in stratocumulus clouds

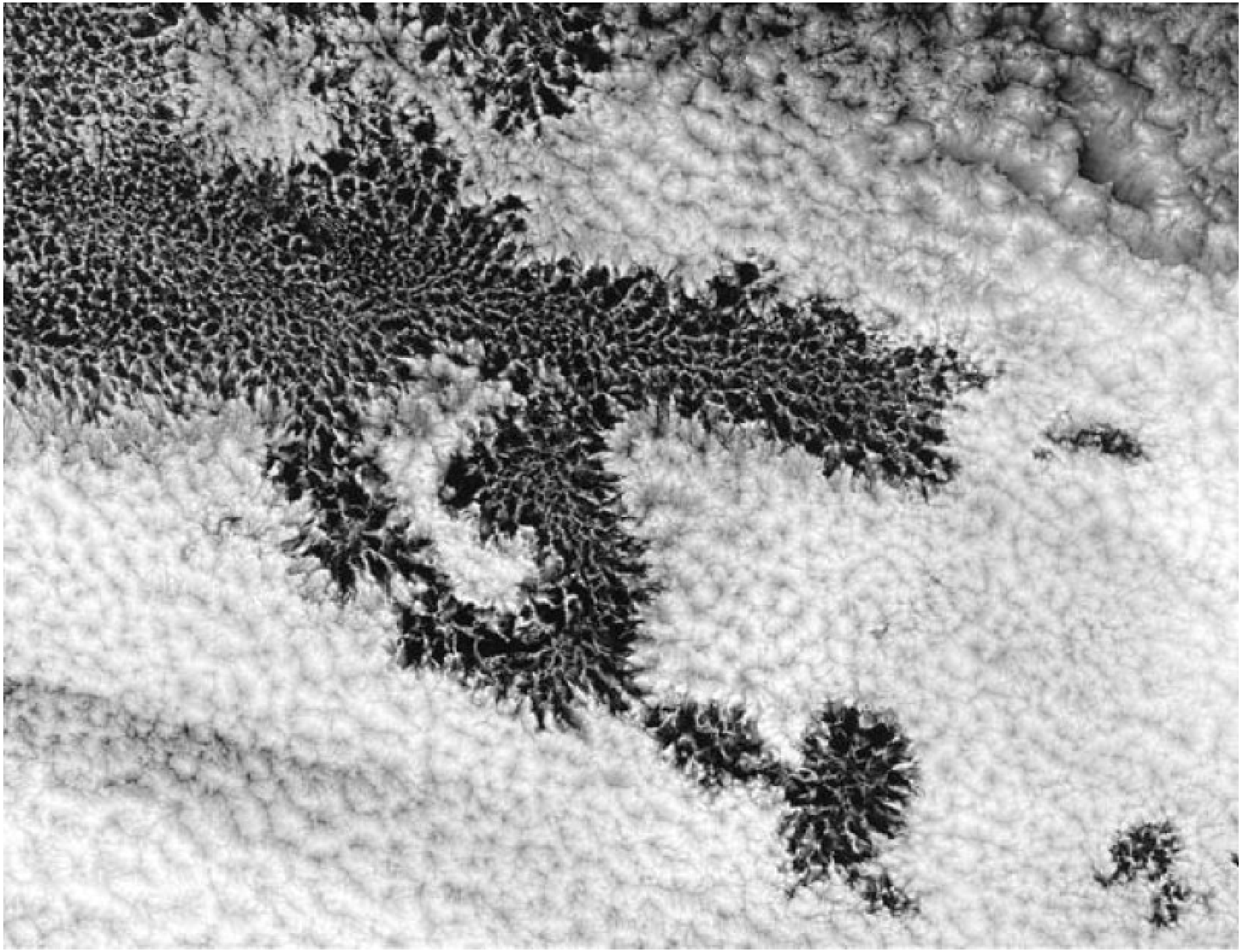

Pockets and Open cells

Stevens et al, 2005

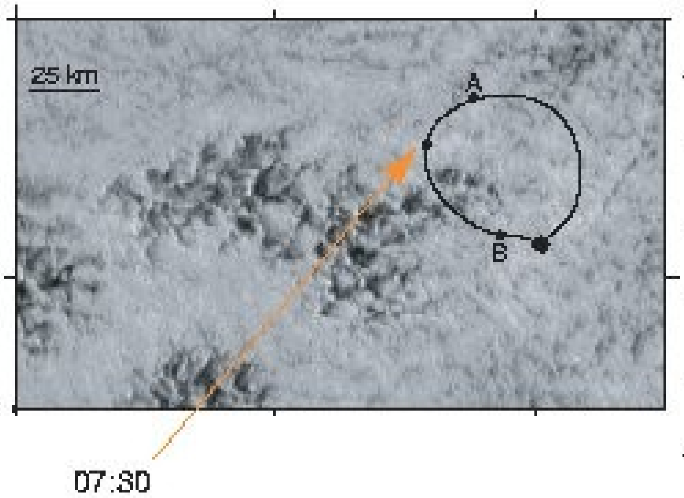

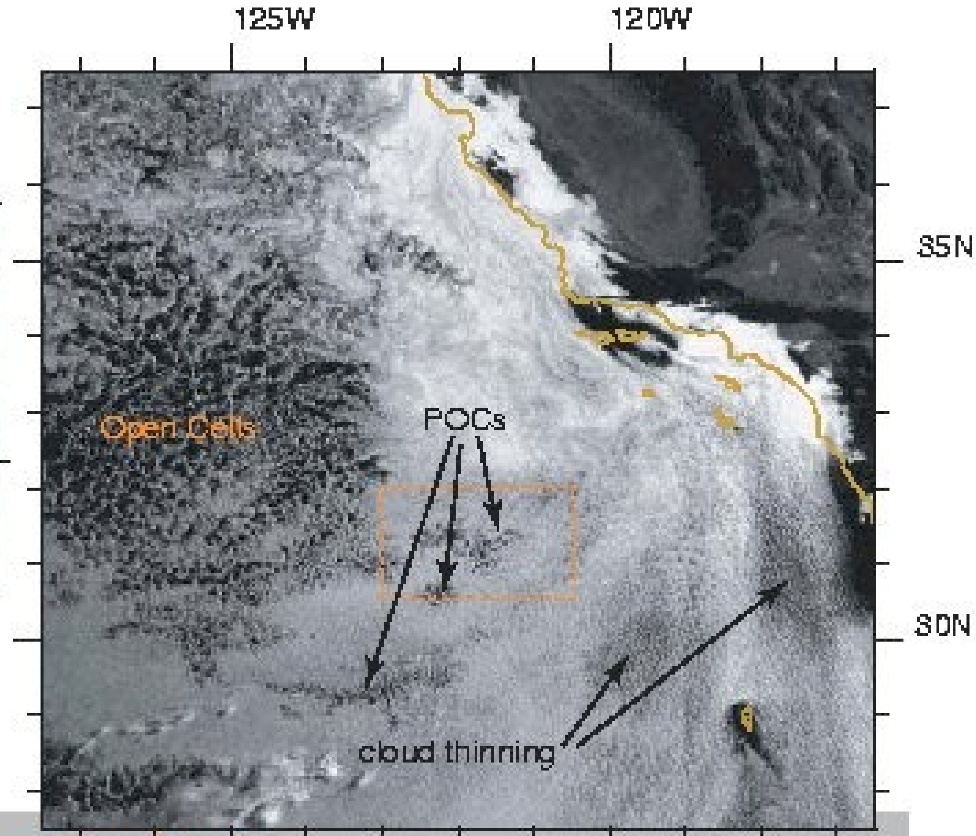

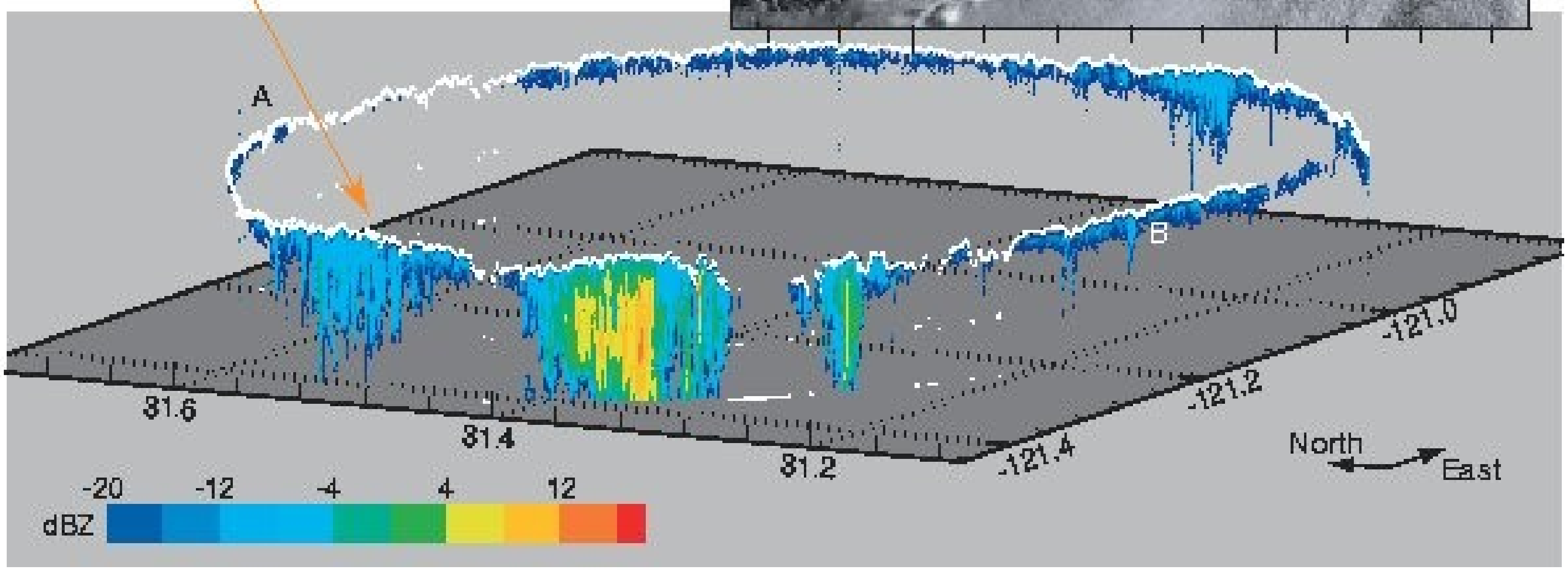

Pockets and Open cells

Van Zanten et al, 2005

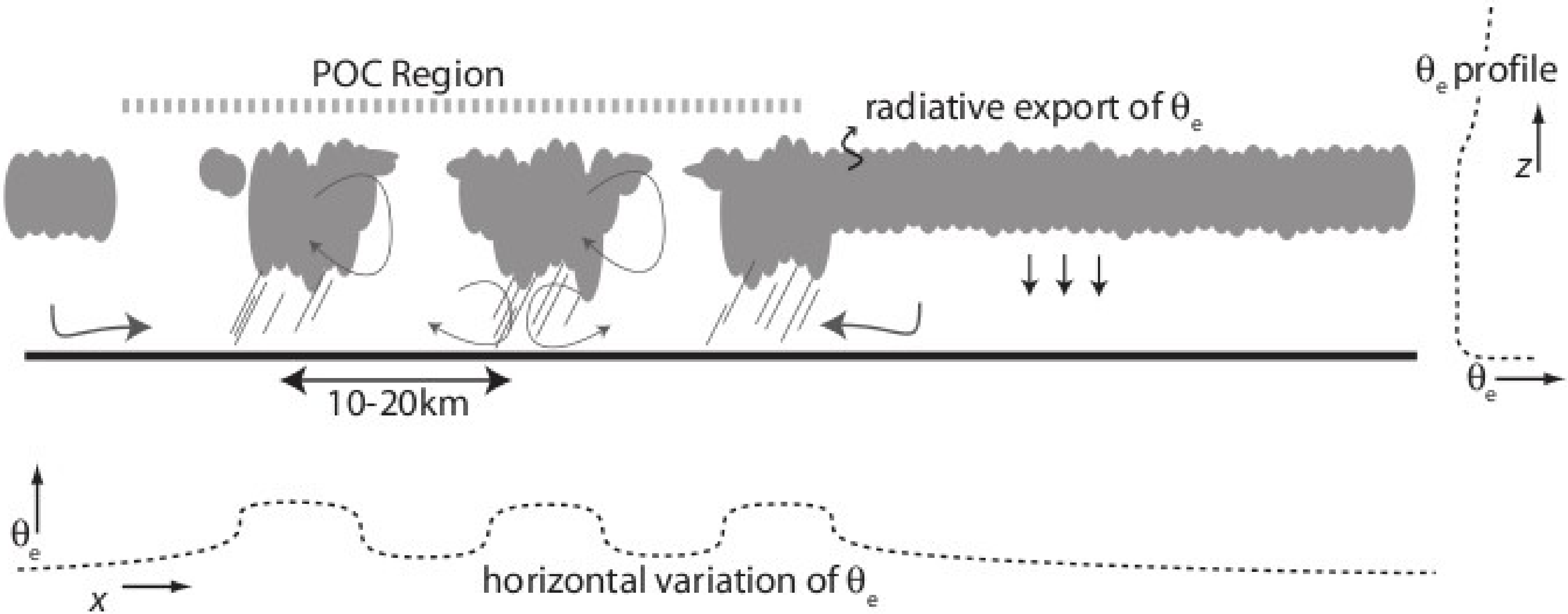

Van Zanten, Stevens et al, 2005

Structure of the Trade Cumuli

Stevens, 2006

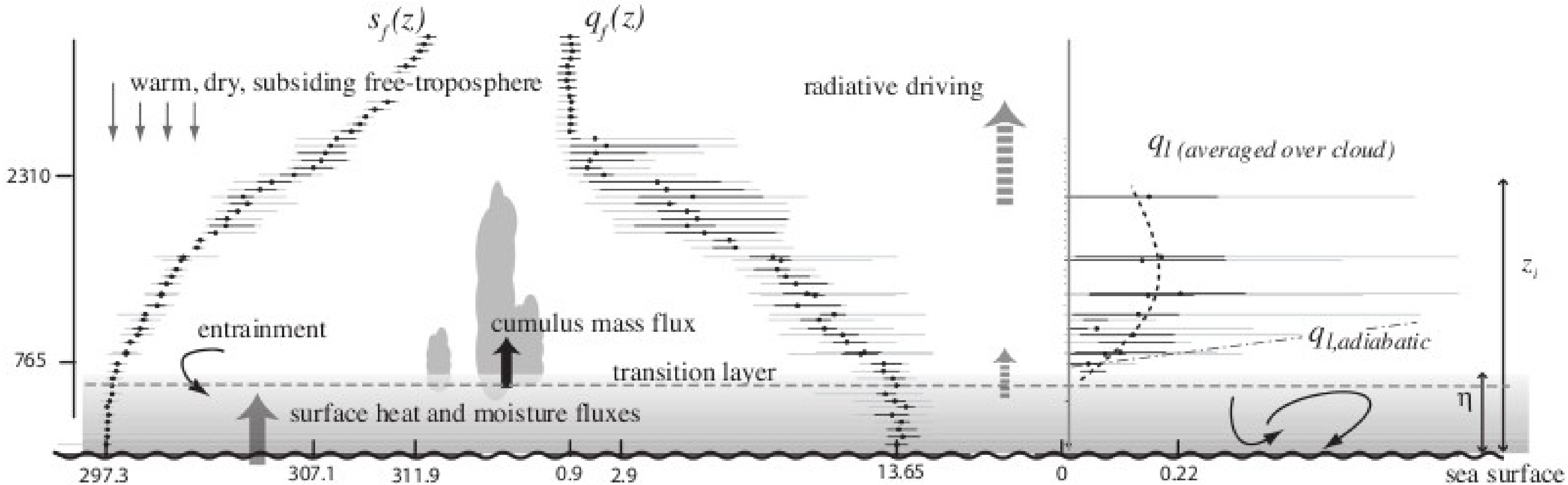

Stevens, 2006

PBL in complex terrain

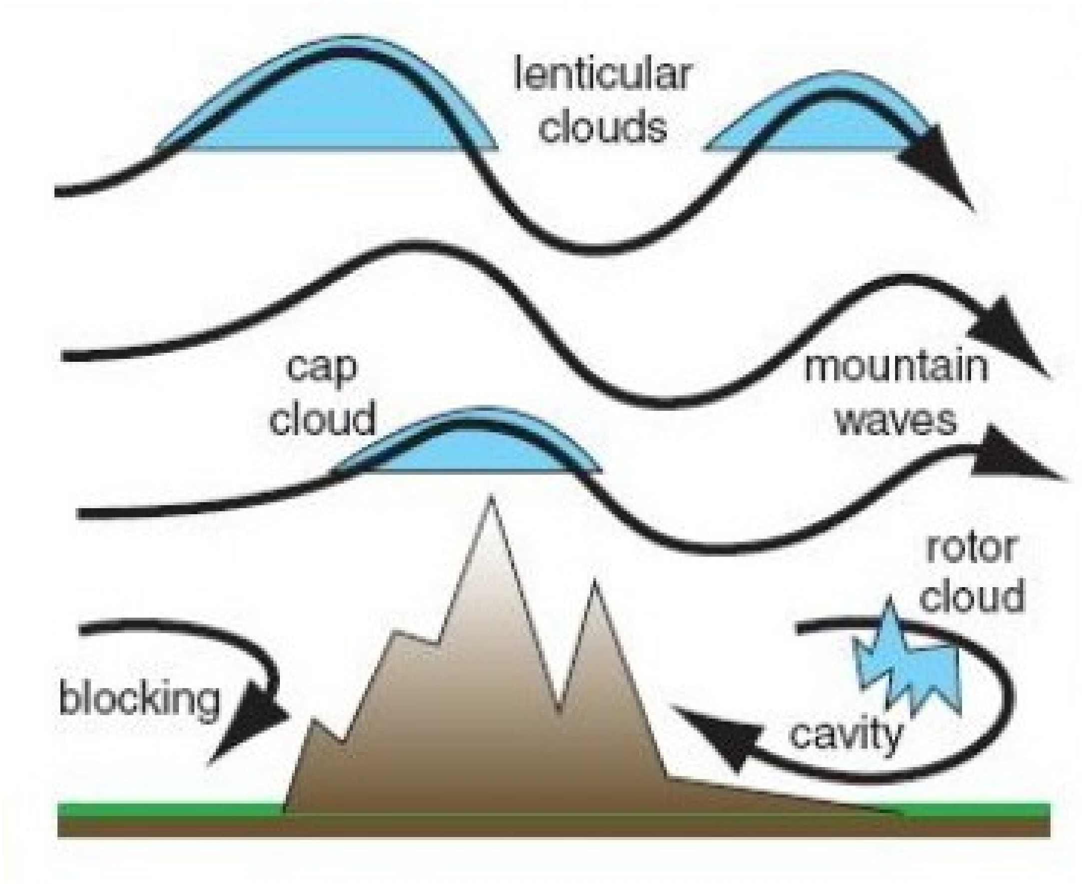

$$F_r = \frac{U}{Nh}$$

$$F_r^* = \frac{U}{N(Z_i - h)}$$

Wallace and Hobbes, 2006


Lenticular cloud
Photo by M.

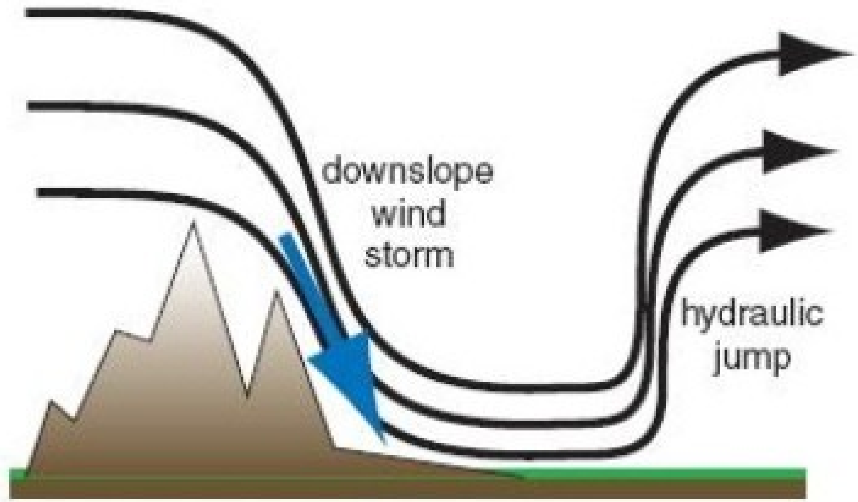

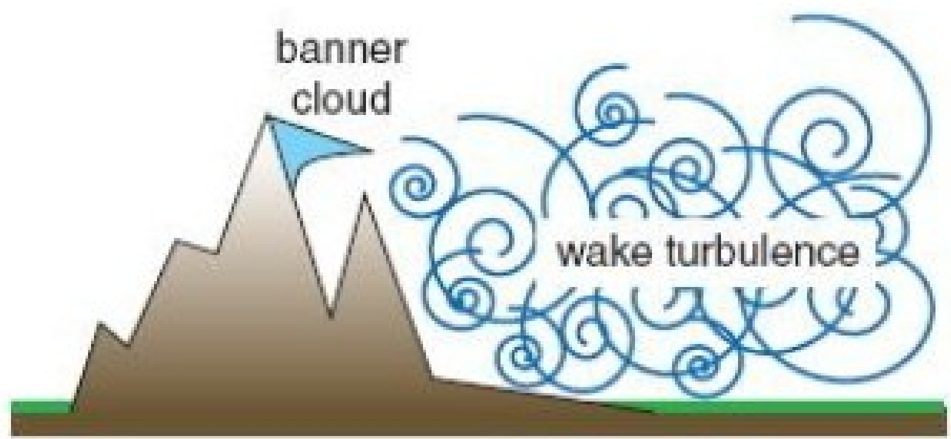

Wallace and Hobbes, 2006

Banner cloud

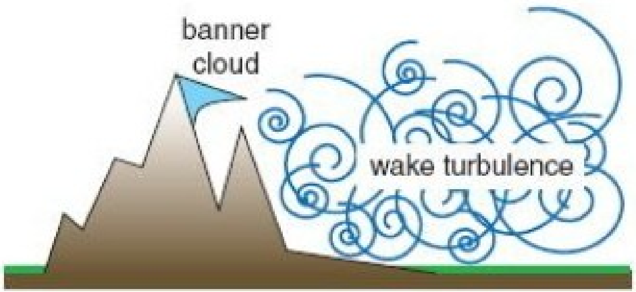

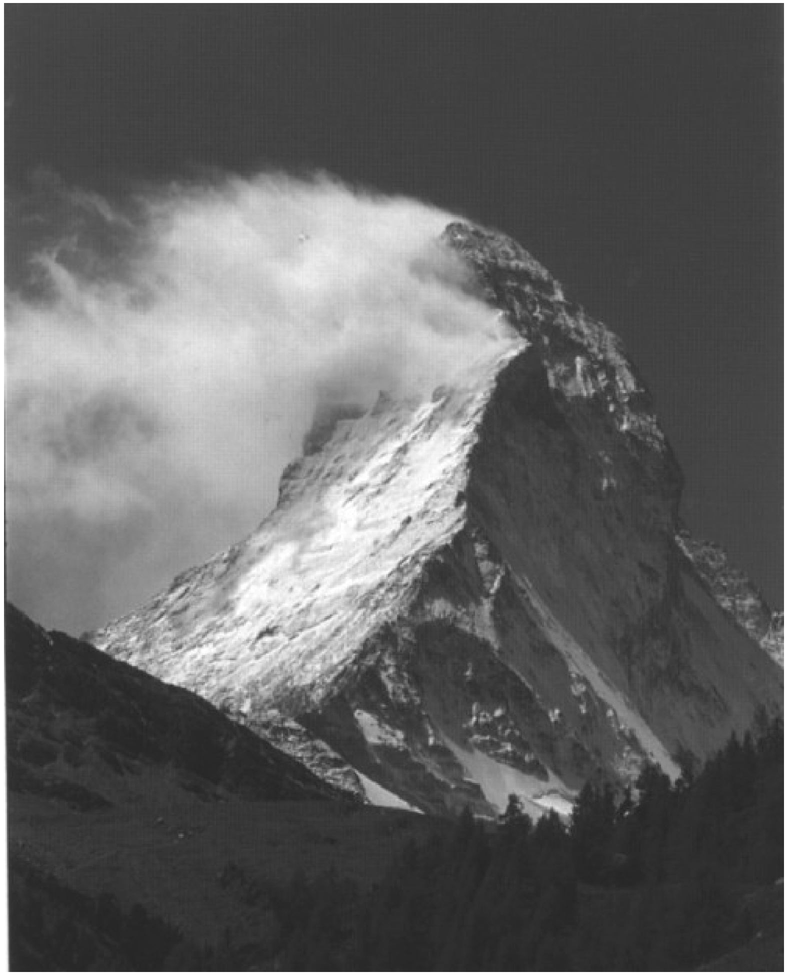

formation of banner clouds

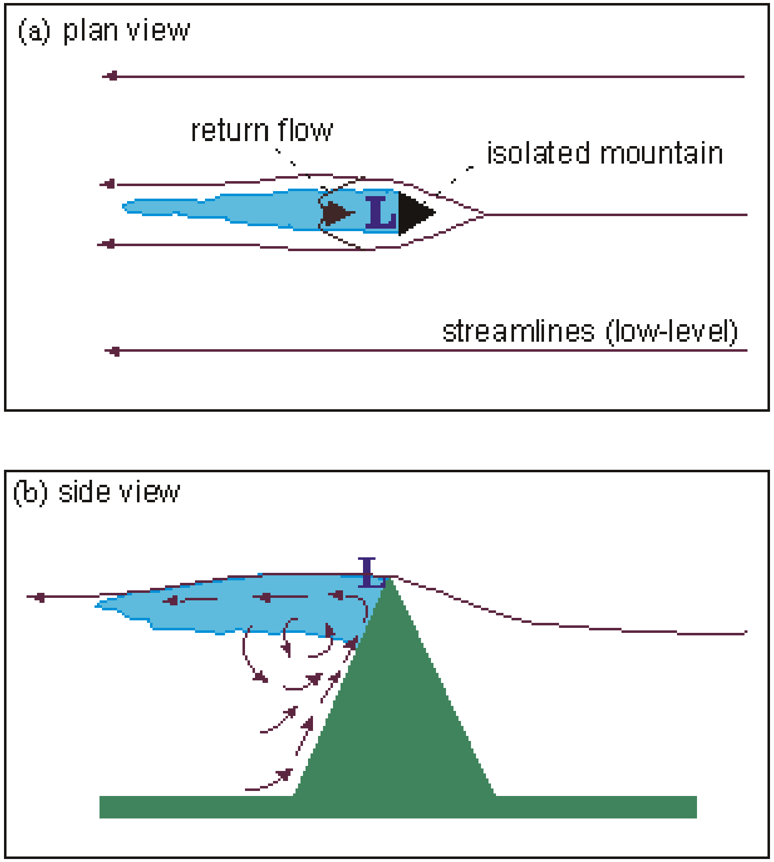

Courtesy of Bart Geers

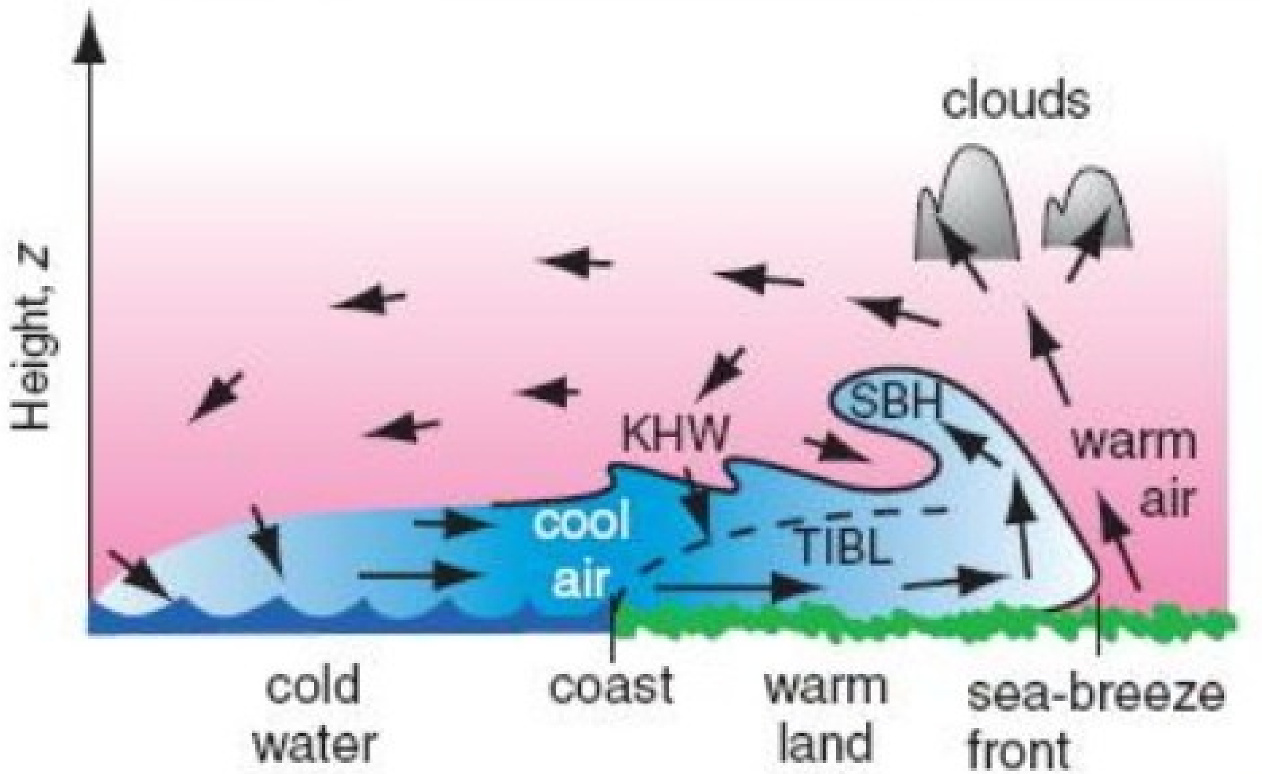

Wallace and Hobbes, 2006

Lecture II – 1h

Probing boundary layer turbulence

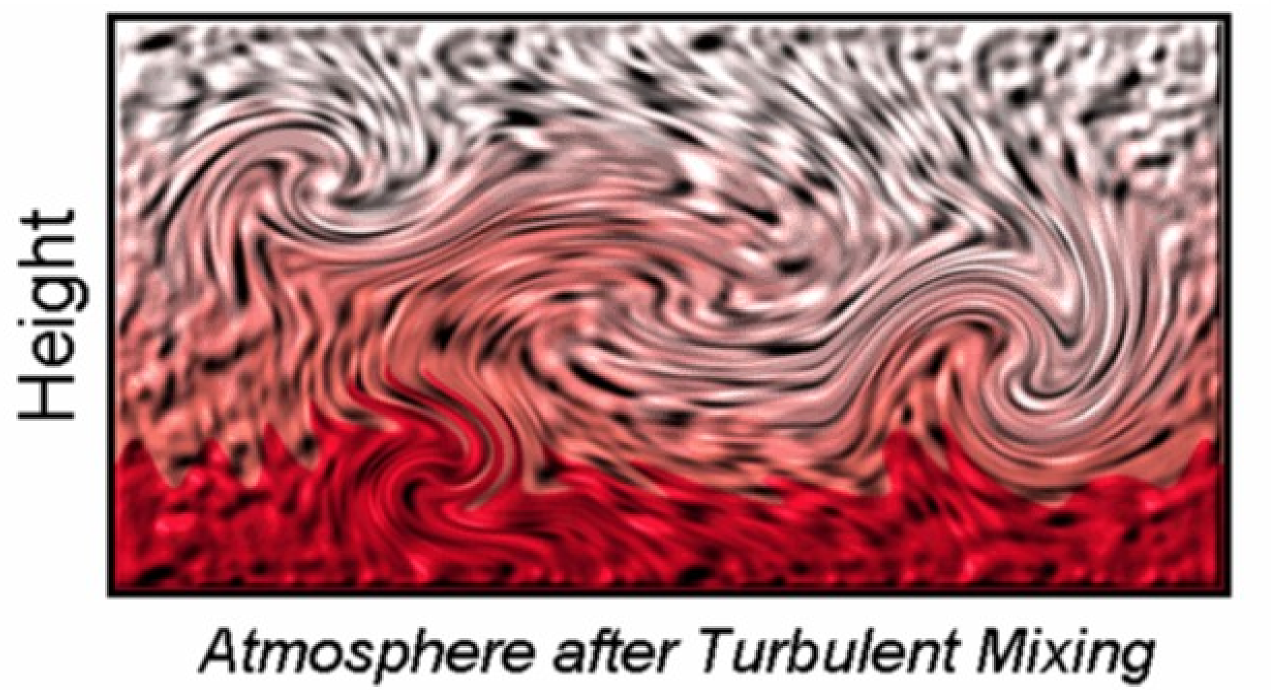

Resolving Navier-Stokes equation with perturbations

$$u = < u > + u'$$

Momentum equations,

$$\frac{\partial < u >}{\partial t} + < u > \frac{\partial < u >}{\partial x} + < v > \frac{\partial < u >}{\partial y} + < w > \frac{\partial < u >}{\partial z} - f < v > = -\frac{1}{\rho}\frac{\partial < p >}{\partial x}$$

$$-\frac{1}{\rho}\left[\frac{\partial < \rho u'u' >}{\partial x} + \frac{\partial < \rho u'v' >}{\partial y} + \frac{\partial < \rho u'w' >}{\partial z}\right] + \nu\nabla^2 < u >,$$

$$\frac{\partial < w >}{\partial t} + < u > \frac{\partial < w >}{\partial x} + < v > \frac{\partial < w >}{\partial y} + < w > \frac{\partial < w >}{\partial z} = -\frac{1}{\rho}\frac{\partial < p >}{\partial z}$$

$$+g\frac{< \theta >}{\theta_0} - \frac{1}{\rho}\left[\frac{\partial < \rho u'w' >}{\partial x} + \frac{\partial < \rho v'w' >}{\partial y} + \frac{\partial < \rho w'w' >}{\partial z}\right] + \nu\nabla^2 < w >,$$

Adiabatic thermodynamics energy equation,

$$\frac{\partial < \theta >}{\partial t} + < u > \frac{\partial < \theta >}{\partial x} + < v > \frac{\partial < \theta >}{\partial y} + < w > \frac{\partial < \theta >}{\partial z} = - < w > \frac{d\theta_0}{dz}$$

$$+\left[\frac{\partial < u'\theta' >}{\partial x} + \frac{\partial < v'\theta' >}{\partial y} + \frac{\partial < w'\theta' >}{\partial z}\right],$$

A possible closure:

$$< u'w' >= -K_m \frac{\partial < u >}{\partial z}, < v'w' >= -K_m \frac{\partial < v >}{\partial z}$$

and

$$< \theta' w' >= -K_h \frac{\partial < \theta >}{\partial z},$$

>> Importance of measuring turbulent variables,
To check, suggest and improve parameterizations

Probing turbulence from the ground

Figure 3.1: Taylor's hypothesis (Stull 1988)

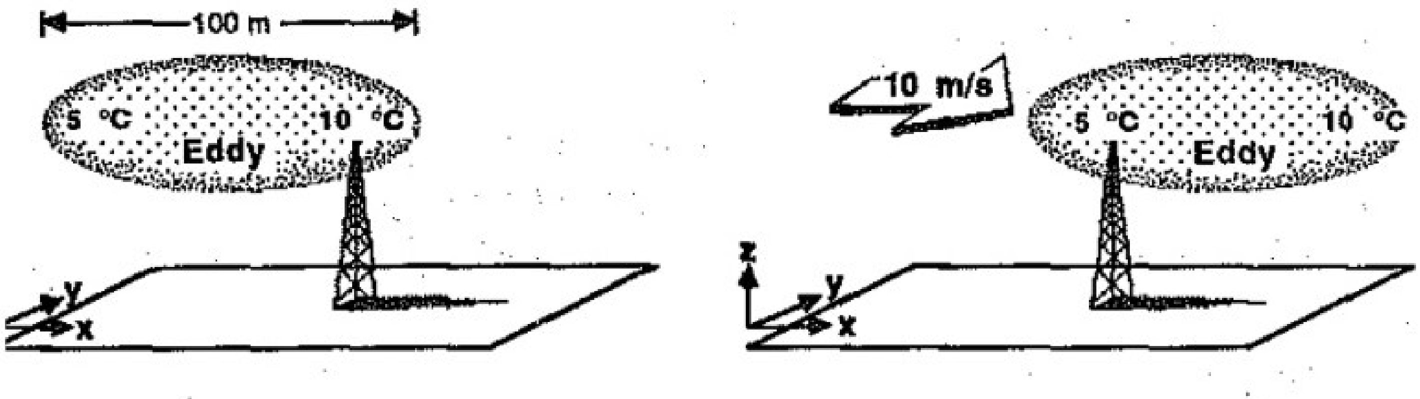

$$\frac{d\xi}{dt} = 0$$

$$\frac{\partial \xi}{\partial t} + \vec{U} \cdot \vec{\nabla} \xi = 0$$

$$\frac{\partial \xi}{\partial t} = -u\frac{\partial \xi}{\partial x} - v\frac{\partial \xi}{\partial y} - w\frac{\partial \xi}{\partial z}$$

Distance/time/frequency equivalence

$$d = U\,t$$

$$k = \frac{2\pi\,\nu}{U}$$

Probing turbulence from an aircraft

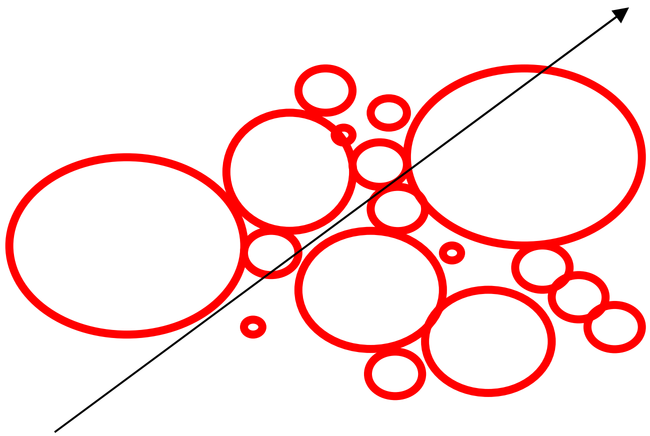

Distance/time equivalence

$$d = U_a t$$

$$k = \frac{2\pi \nu}{U_a}$$

U_a *: Airplane True Airspeed*

! *Concepts of « Transverse » and « Longitudinal » are different than*
when measuring from the ground !

In situ measurements of the air motion with an aircraft

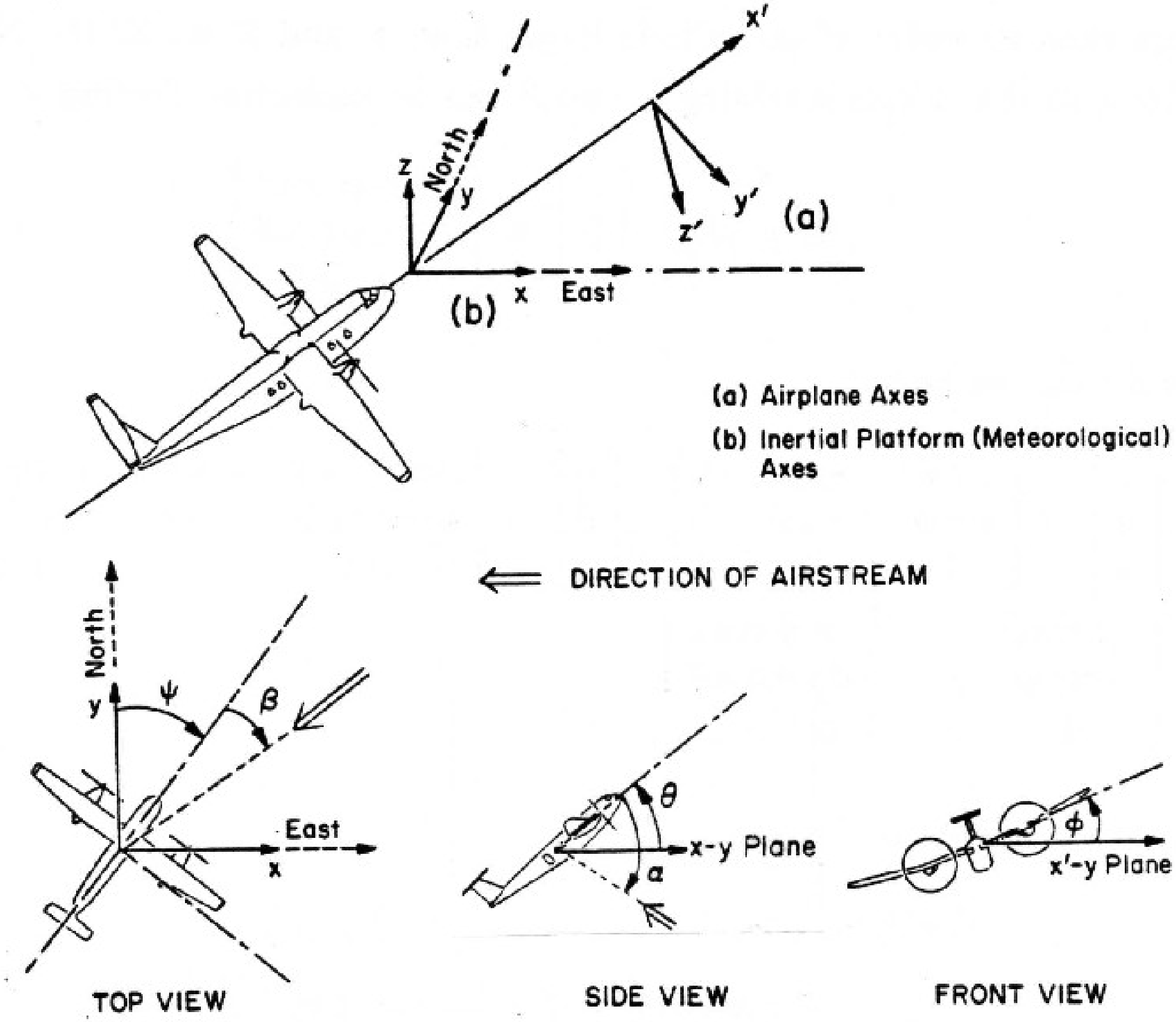

~100 m/s

$$\vec{v} = \vec{v}_p + \vec{v}_a$$

↓ (approx.)

$$u = -U_a \sin(\psi + \beta) + u_p$$

$$v = -U_a \cos(\psi + \beta) + v_p$$

$$w = -U_a \sin(\theta - \alpha) + w_p$$

~1 m/s ~100 m/s ~0.01 ~1 m/s

Lenschow, RAF Bulletin #23

Definition and measurements of PBL turbulent processes

Content:

- Statistics
- Integral scales
- Fluxes
- Entrainment
- Turbulent kinetic energy
- Higher-order moments

Example of measured air vertical velocity time series

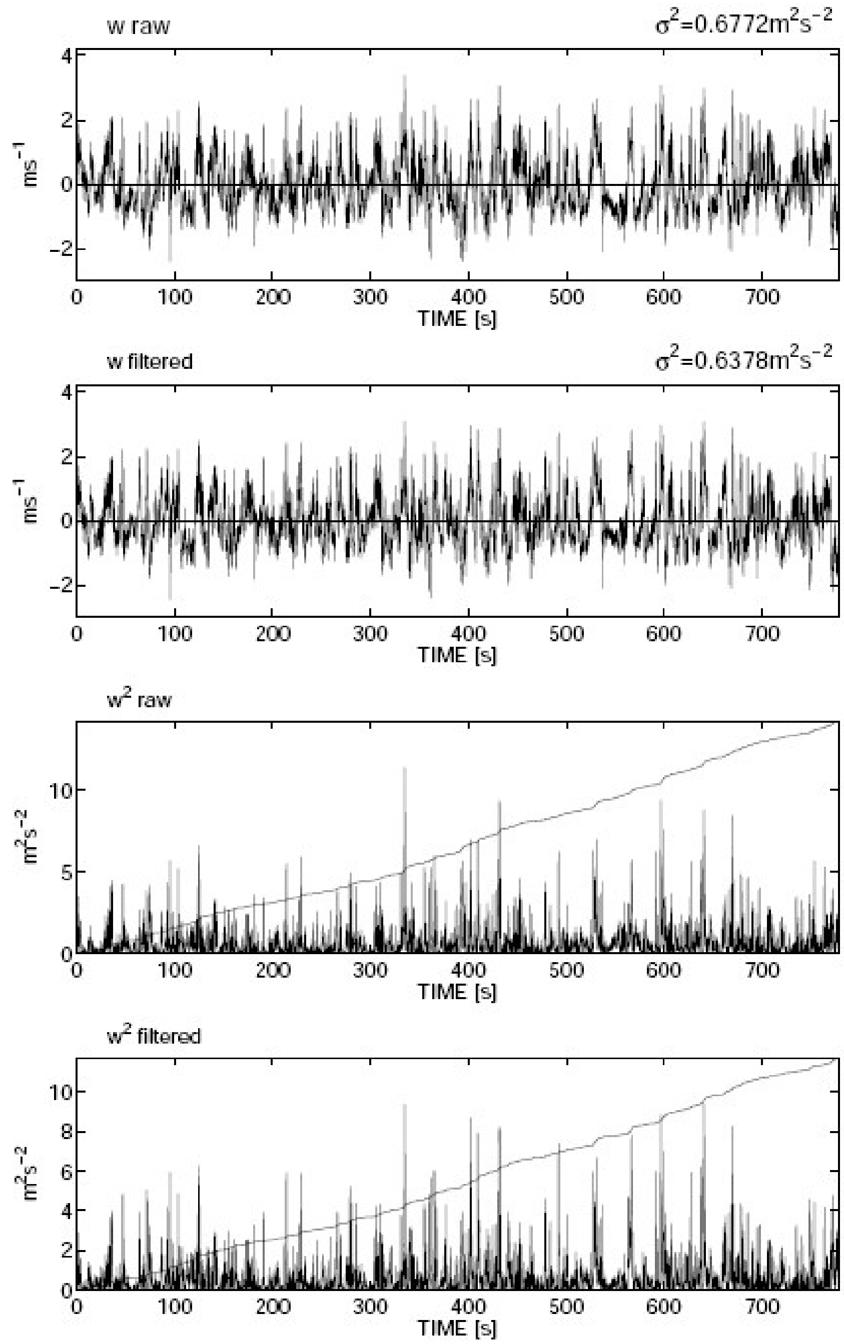

Figure 1: Air vertical velocity component (w) timeseries. Raw/filtered ratio=1.062

Example of measured air temperature time series

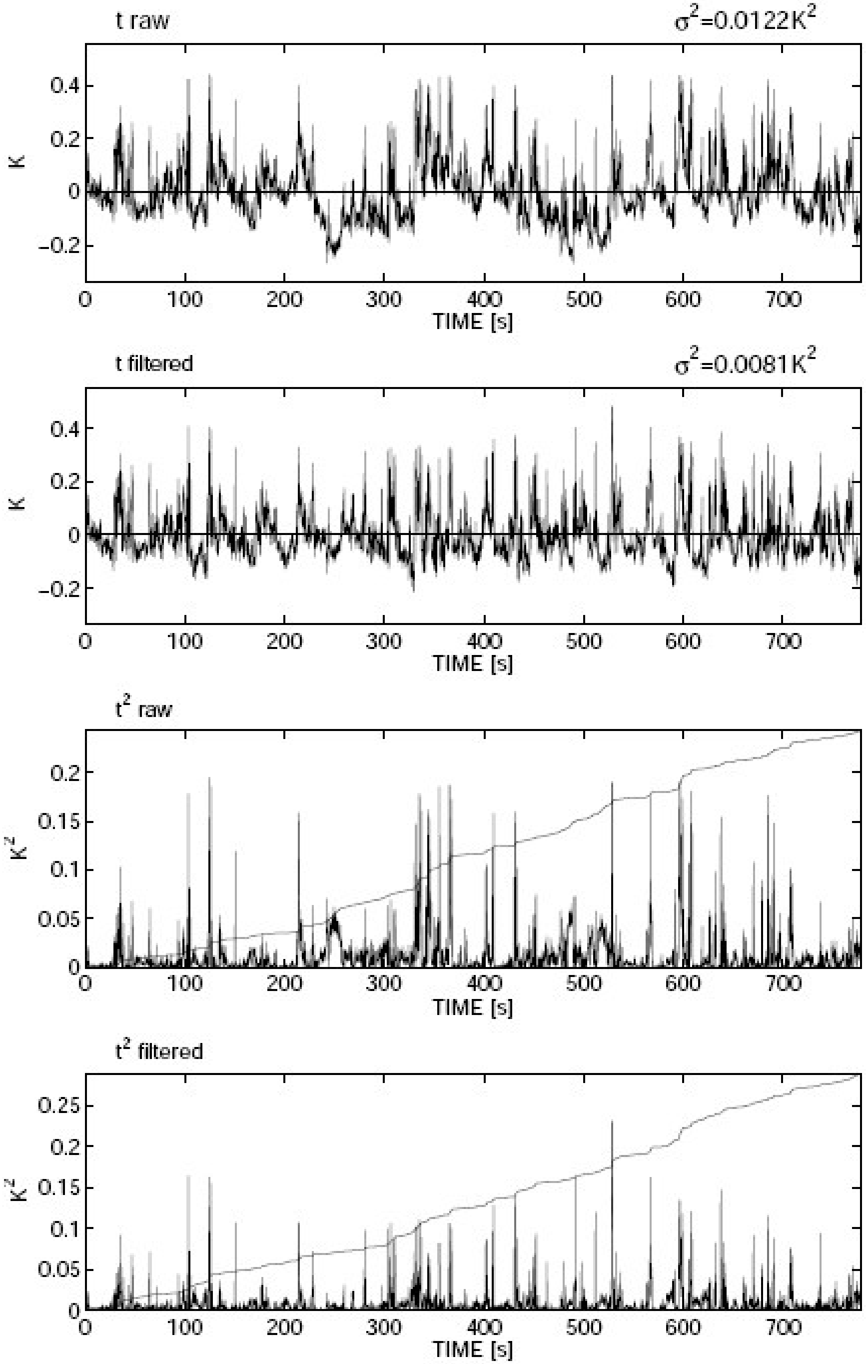

Figure 2: Temperature (t) timeseries. Raw/filtered ratio=1.493

Statistical approach

$$\sigma_\xi^2 = \frac{1}{(N-1)}\sum_{i=0}^{N-1}(\xi_i - \overline{\xi})^2$$

If N is large enough $\left(\frac{1}{(N-1)} \cong \frac{1}{N}\right)$, the variance will be:

$$\sigma_\xi^2 = \frac{1}{N}\sum_{i=0}^{N-1}(\xi_i - \overline{\xi})^2$$

Substituting $\xi_i = \overline{\xi}_i + \xi_i^{'}$:

$$\sigma_\xi^2 = \frac{1}{N}\sum_{i=0}^{N-1}(\xi_i^{'})^2 = \overline{(\xi^{'})^2}$$

$$\text{covar}(\xi,\varsigma) = \frac{1}{N}\sum_{i=0}^{N-1}(\xi_i - \overline{\xi_i})\cdot(\varsigma_i - \overline{\varsigma_i}) = \frac{1}{N}\sum_{i=0}^{N-1}(\xi_i^{'}\varsigma_i^{'}) = \overline{\xi^{'}\varsigma^{'}}$$

$$\text{r}_{\xi\varsigma} = \frac{\overline{\xi^{'}\varsigma^{'}}}{\sigma_\xi \sigma_\varsigma}$$

Higher-order moments

Variance $\sigma_w^2 = \langle w'^2 \rangle$

$\mu_3 = \langle w'^3 \rangle$

$\mu_4 = \langle w'^4 \rangle$

$S = \dfrac{\mu_3}{\sigma^3}$ Skewness

$K = \dfrac{\mu_4}{\sigma^4}$ Kurtosis

INTEGRAL SCALES

The **autocovariance function** of vertical velocity w is defined as

$$R_w(r) \equiv \int_{-\infty}^{\infty} w(r')w(r'+r)dr', \tag{1}$$

where r is the displacement. The **integral scale**, which is a measure of the length over which w is relatively well correlated with itself, is defined as

$$l_w = \int_0^{\infty} \frac{R_w(r)}{R_w(0)} dr. \tag{2}$$

l_w can be estimated from the maximum of the running integral of (2):

$$l_w(r) \cong \left[\int_0^{r} \frac{R_w(r')}{R_w(0)} dr' \right]_{max}, \tag{3}$$

which is reached at the first zero crossing of $R_w(r)$.

Integral scale

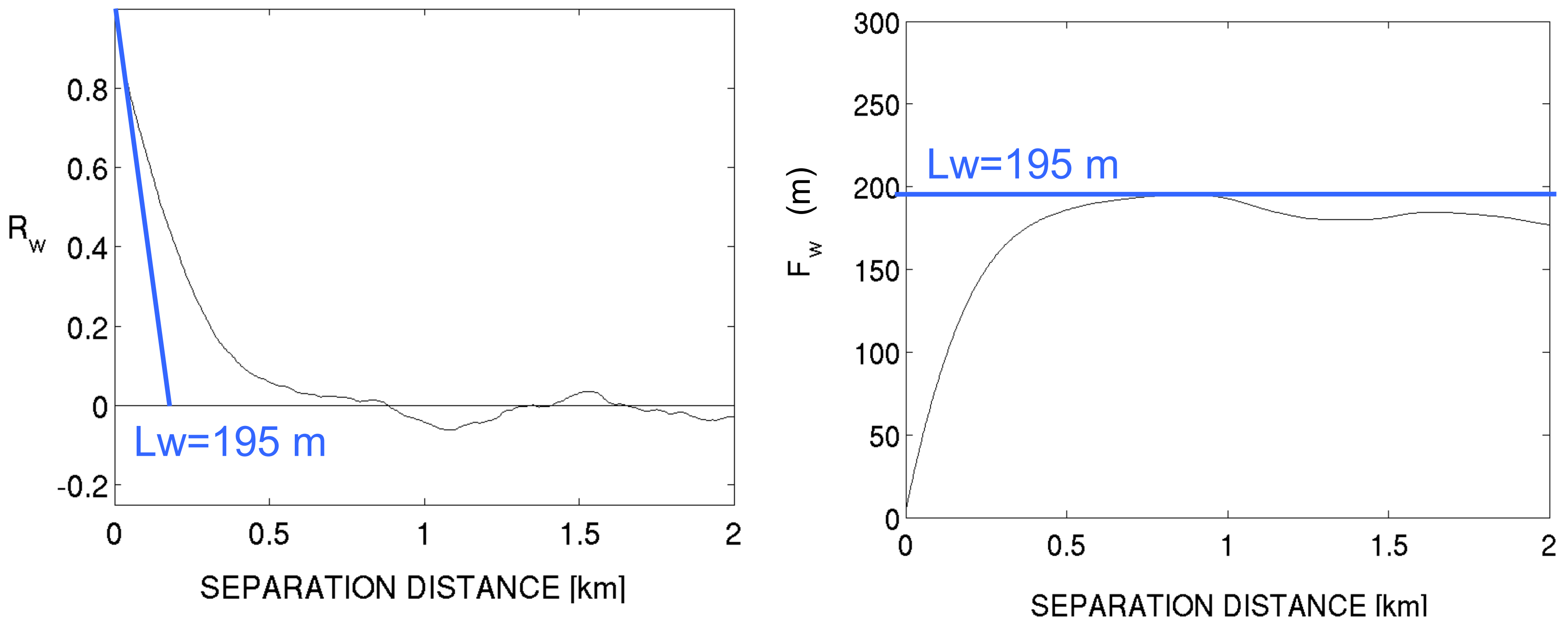

Energy density spectrum

Vertical velocity energy spectrum

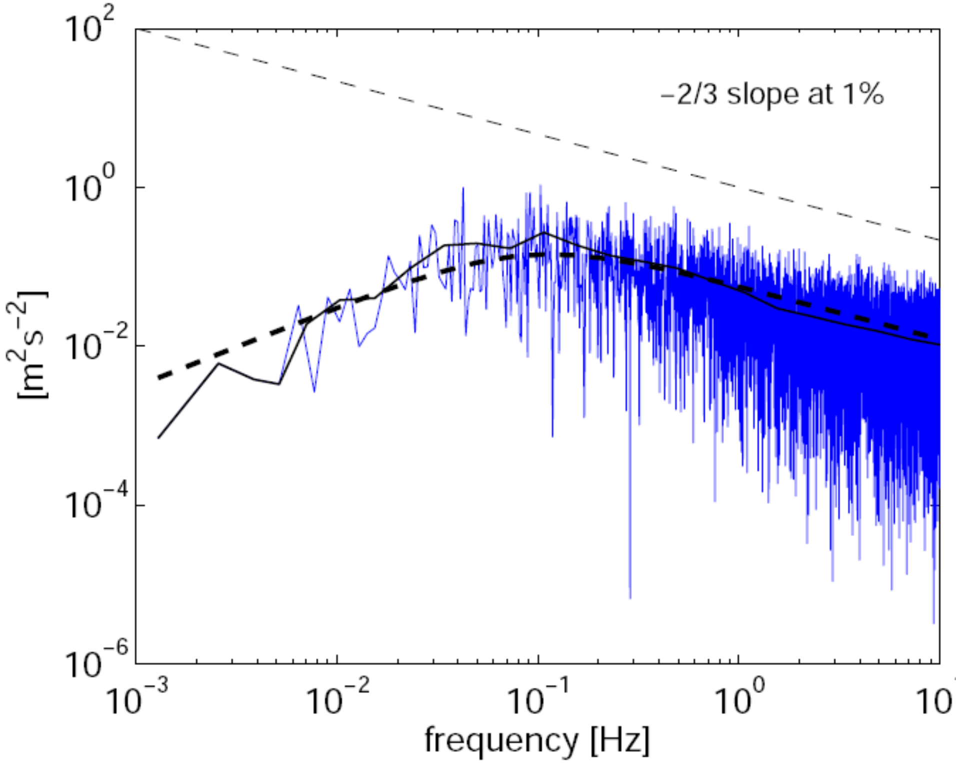

$$F_w(f) = FFT(w(t))$$

$$S_w(f) = F_w(f) F_w^*(f)$$

$$S_w(f) = FFT(R_w(\tau))$$

$$R_w(\tau) = IFFT(S_w(f))$$

Turbulent Kinetic Energy

$$\bar{e} = \frac{1}{2}\left(\sigma_u^{\;2} + \sigma_v^{\;2} + \sigma_w^{\;2}\right)$$

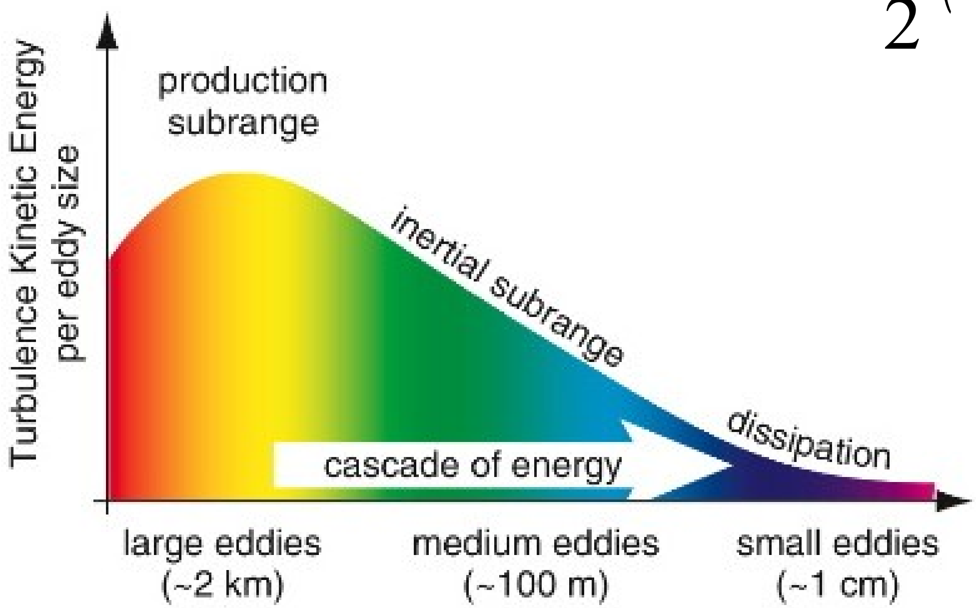

Stull, 1988
Wallace and Hobbes, 2006

$$S_w(k) = \frac{4}{3}\alpha\ \varepsilon^{2/3} k^{-5/3}$$

Kolmogorov constant (α)

Dissipation rate (ε; units: $m^2 s^{-3}$)

Wave number (k)

$$\frac{\partial \overline{e}}{\partial t} = \frac{g}{\overline{\theta_v}}\overline{w'\theta_v'} - \left(\overline{w'u'}\frac{\partial \overline{u}}{\partial z} + \overline{w'v'}\frac{\partial \overline{v}}{\partial z}\right) - \frac{\partial \overline{w'e'}}{\partial z} - \frac{1}{\overline{\rho_0}}\frac{\partial \overline{w'p'}}{\partial z} - \epsilon$$

Production terms (buoyancy and shear) — transport — pressure — dissipation

Sampling errors

$$F = \lim_{T\to\infty} \frac{1}{T}\int_0^\infty w'(t)s'(t)dt \equiv \frac{1}{N}\sum_{i=0:N} w'(i)s'(i)$$

Systematic error ~10%

Associated for example with limited leg or high pass filtering

$$F - \langle F(L) \rangle \approx \frac{2F\mathcal{L}_{ws}}{L}$$

Random error 10 to >50%

$$\frac{\sigma_F(T)}{|F|} \simeq \left(\frac{2\mathcal{T}_f}{T}\right)^{1/2}\left(\frac{1+r_{ws}^2}{r_{ws}^2}\right)^{1/2}$$

Instrumental error < 5%

Lenschow, 1994
Mann and Lenschow, 1994

Kinematic Fluxes

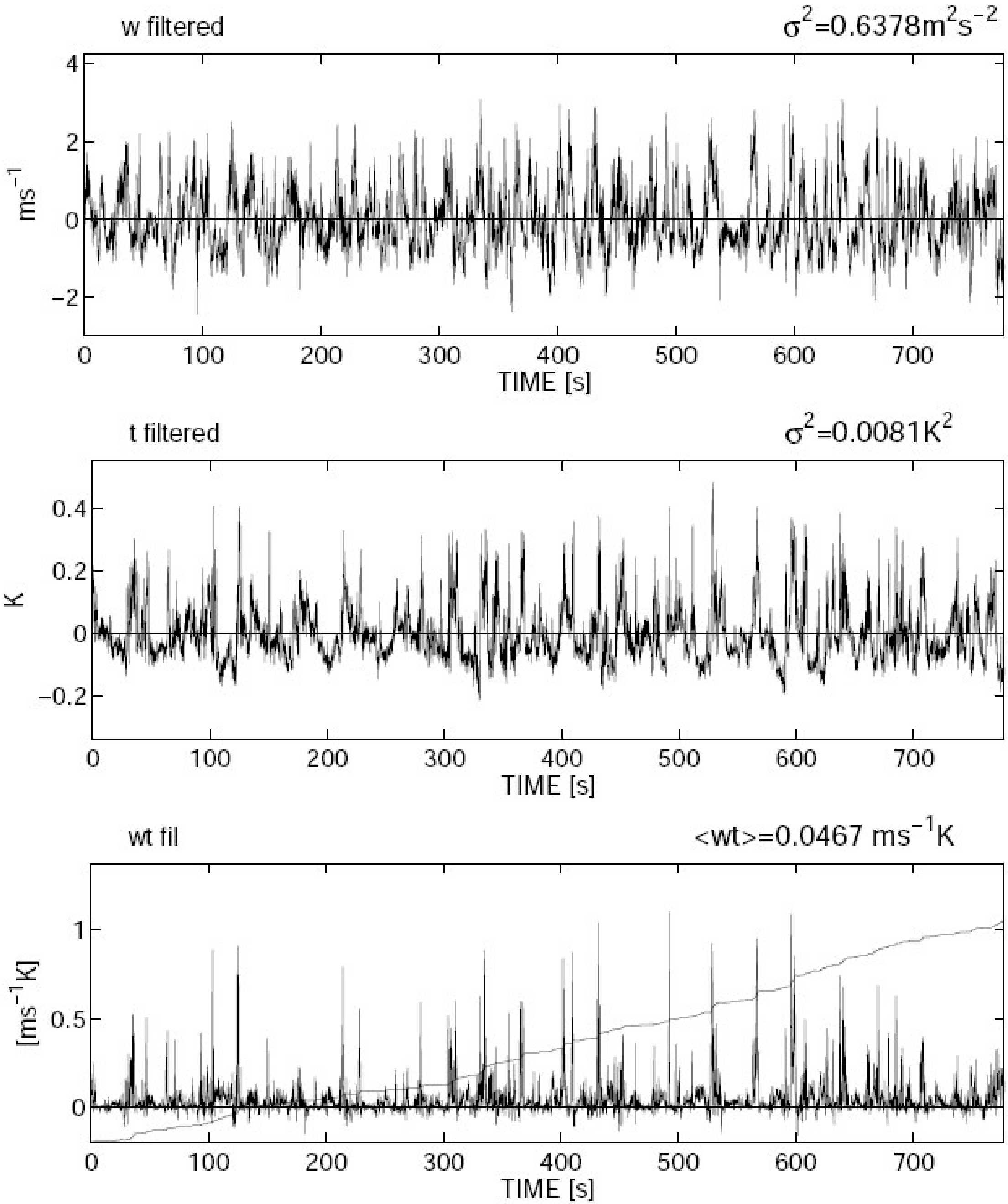

Figure 16: w, t, wt timeseries.

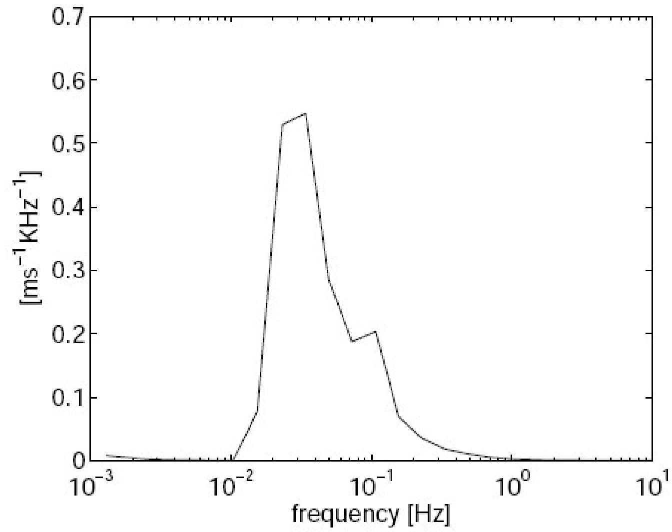

Interpretation of kinematic eddy fluxes (Wallace and Hobbs 2006)

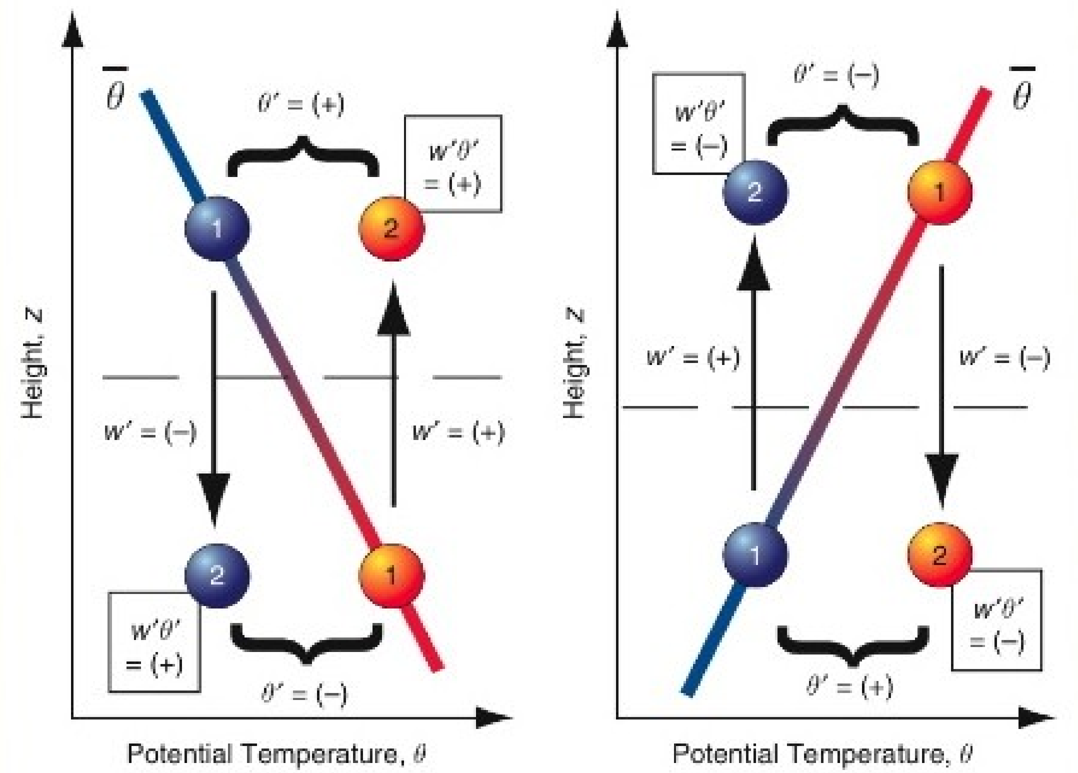

Stull, 1988
Wallace and Hobbes, 2006

Probing the Sahelian boundary layer

Water vapour mixing ratio

Potential temperature

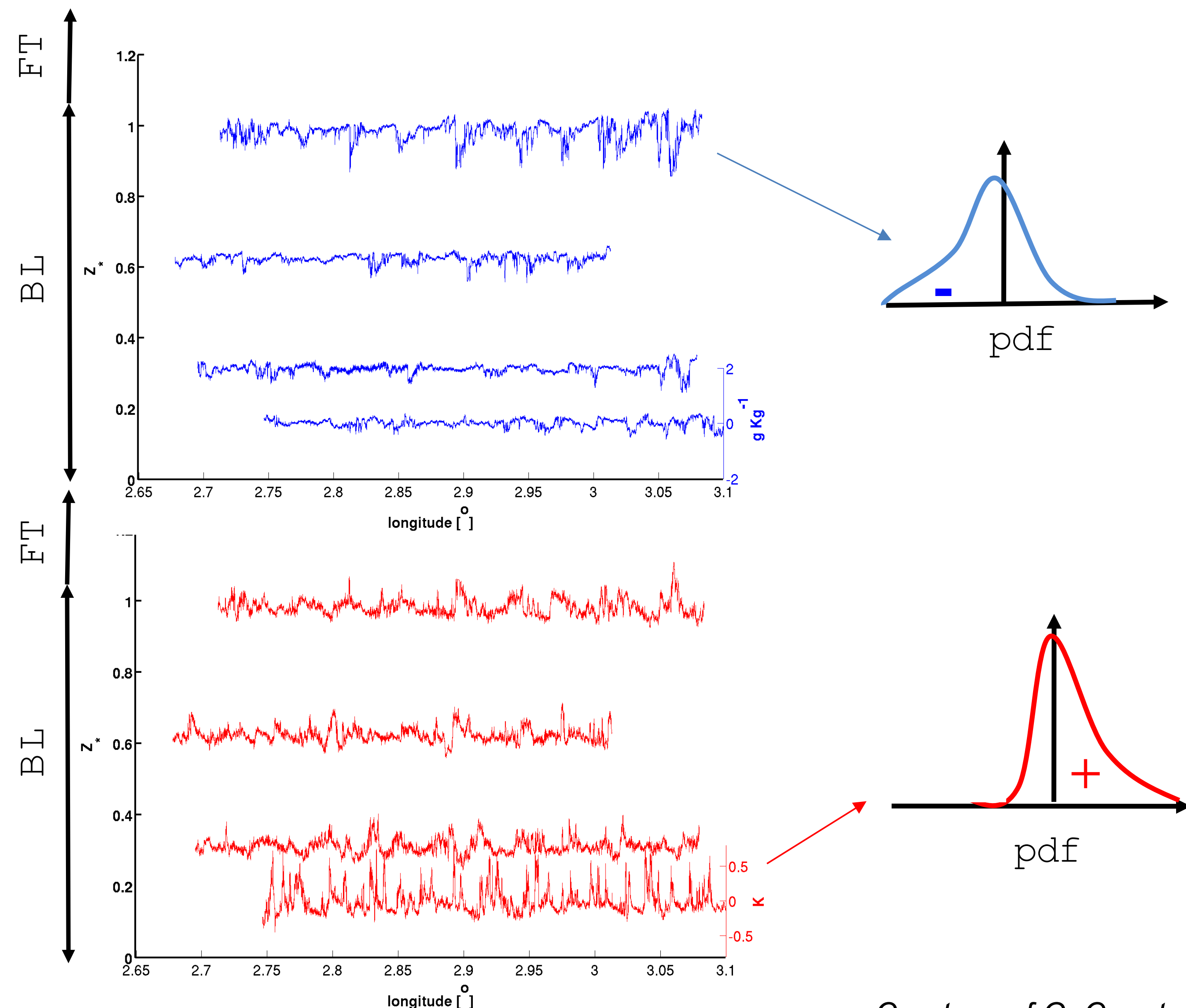

Courtesy of G. Canut, 2010

Cloud edges

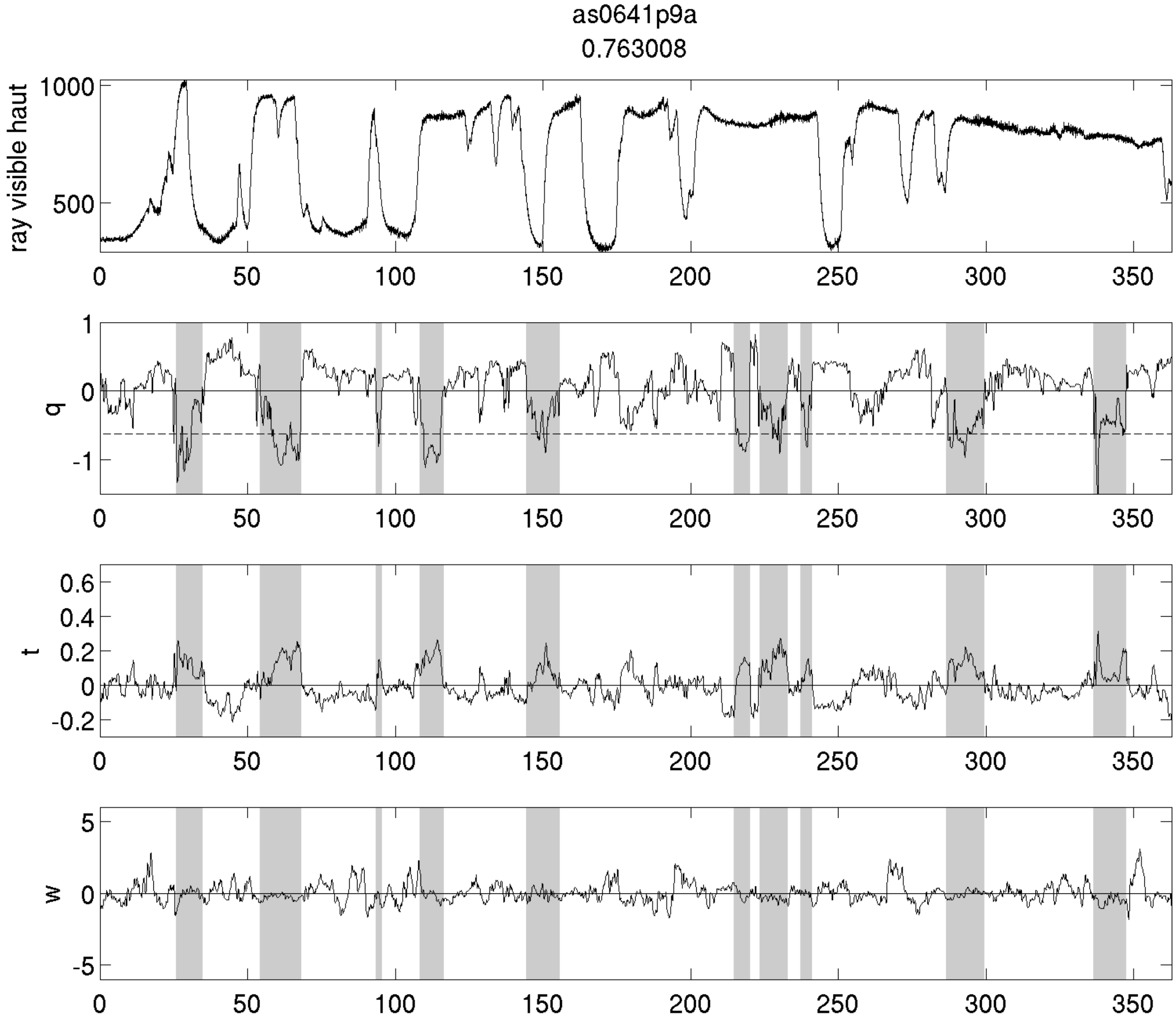
as0641p9a
0.763008
ray visible haut
1000
500
0
50
100
150
200
250
300
350
q
1
0
-1
t
0.6
0.4
0.2
-0.2
w
5
-5

Buoyancy flux vertical structure

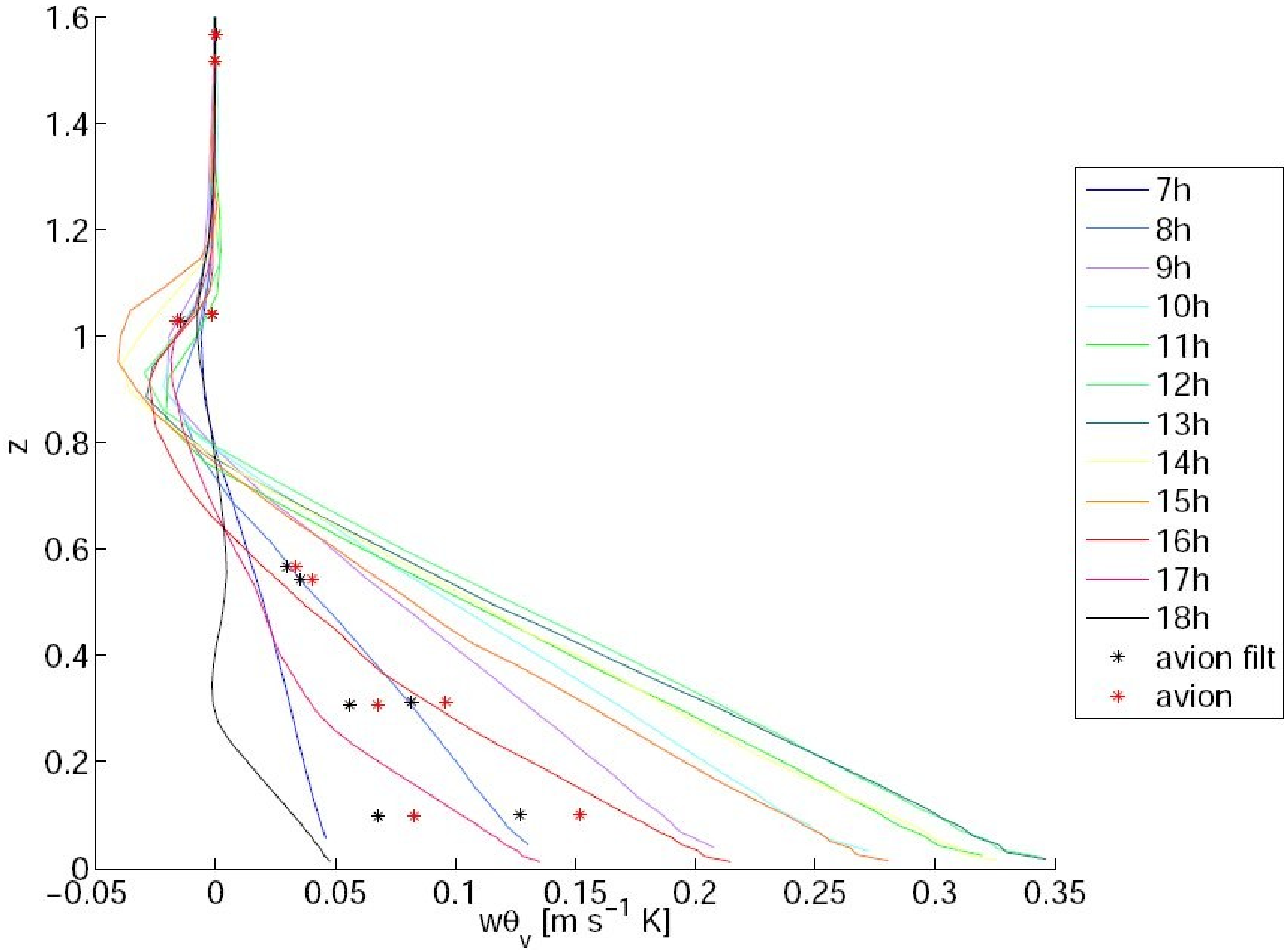

Courtesy of G. Canut, 2010

Vertical profiles of the fluxes in the Sahelian boundary layer

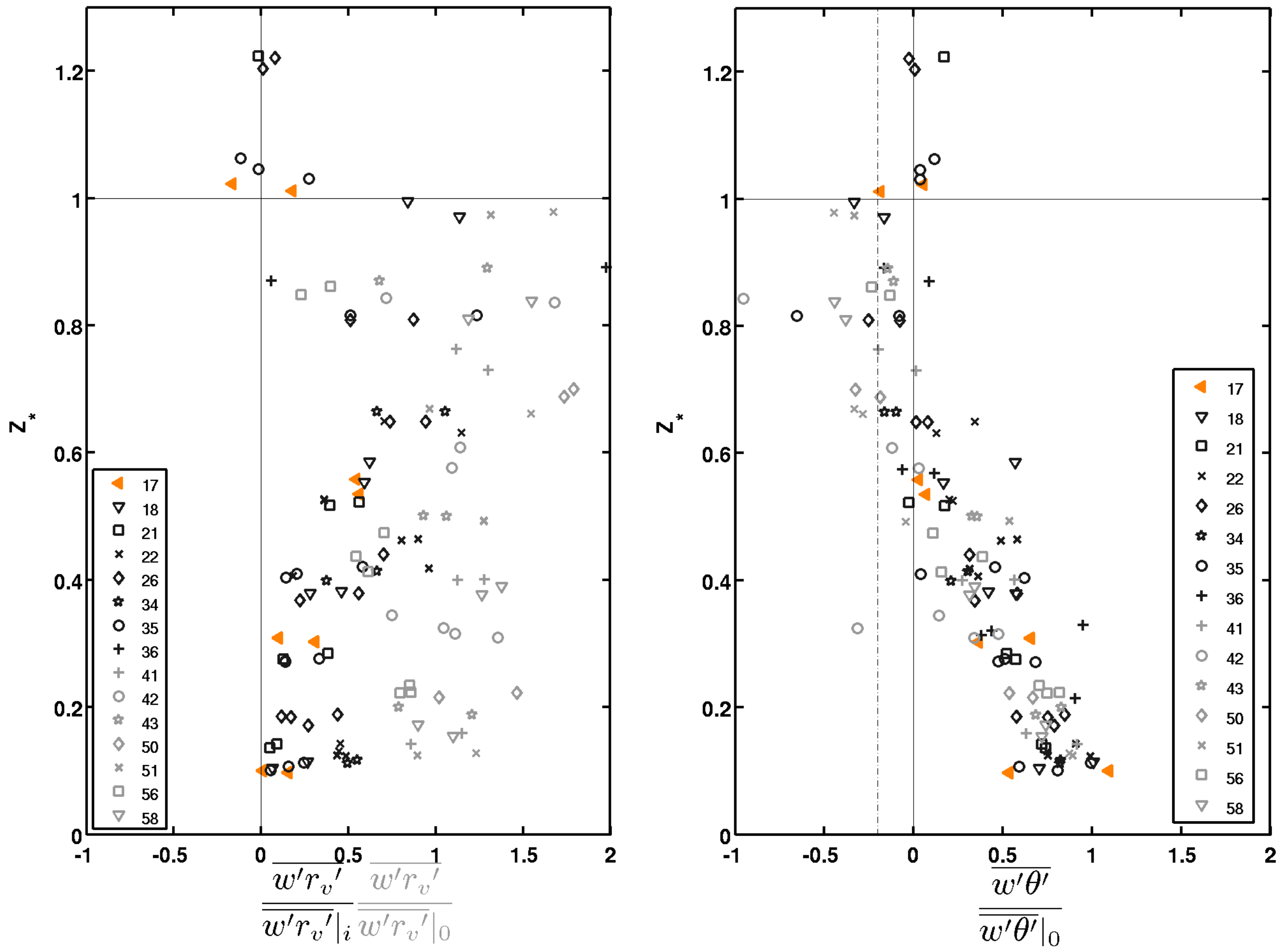

Canut et al, 2010

Boundary layer growth and warming

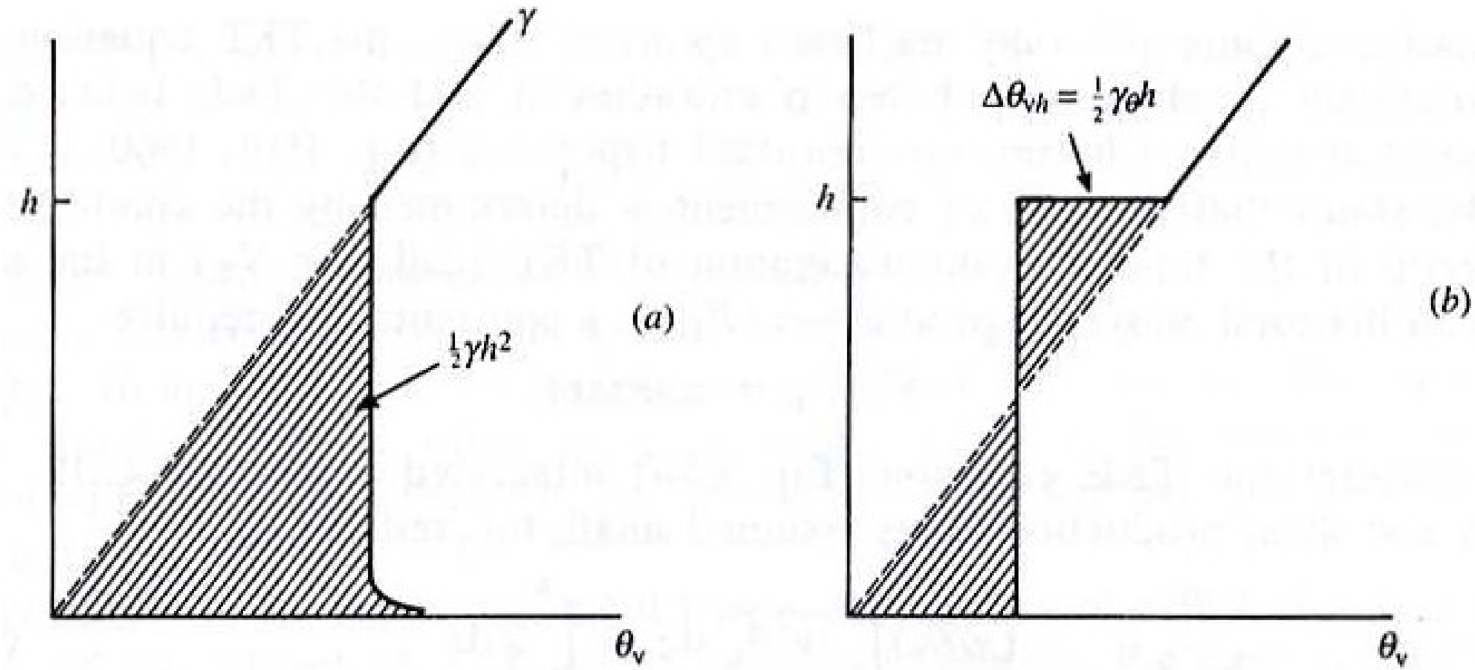

encroachment entrainment

Garratt, 1992

Entrainment rate

$$\beta = -\frac{\overline{w'\theta_v'}|_i}{\overline{w'\theta_v'}|_0}$$

Entrainment velocity

$$w_e = \frac{\partial Z_i}{\partial t} - w_h$$

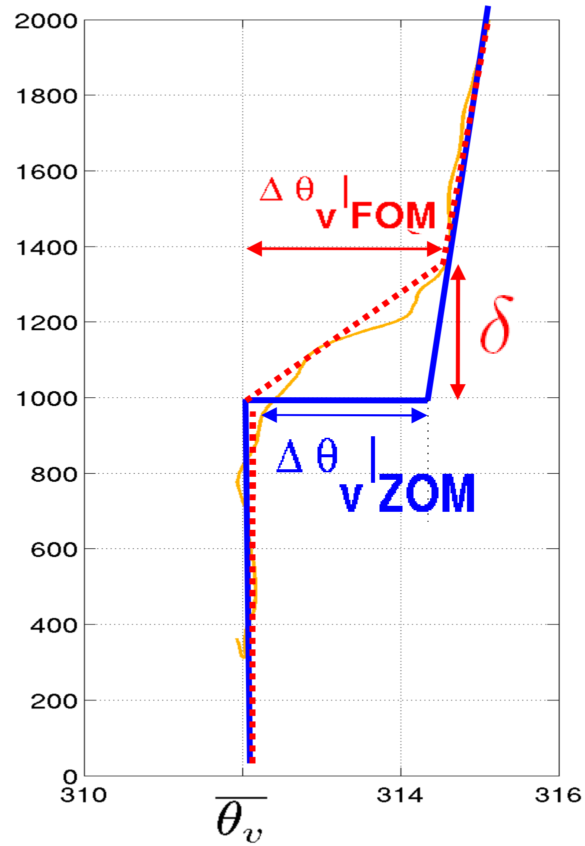

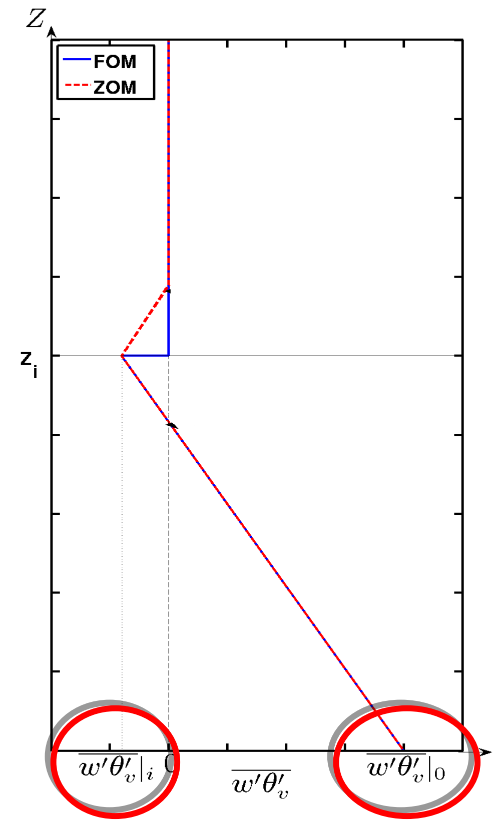

Zero-order model (ZOM)	First-Order Model (FOM)
$w_e \simeq -\frac{\overline{w's'}|_i}{\Delta s}$	$w_e \simeq -\frac{\overline{w's'}|_i}{\Delta s} + \frac{\delta}{\Delta s}\frac{\partial \bar{s}}{\partial t}$

Estimating entrainment from aircraft measurements

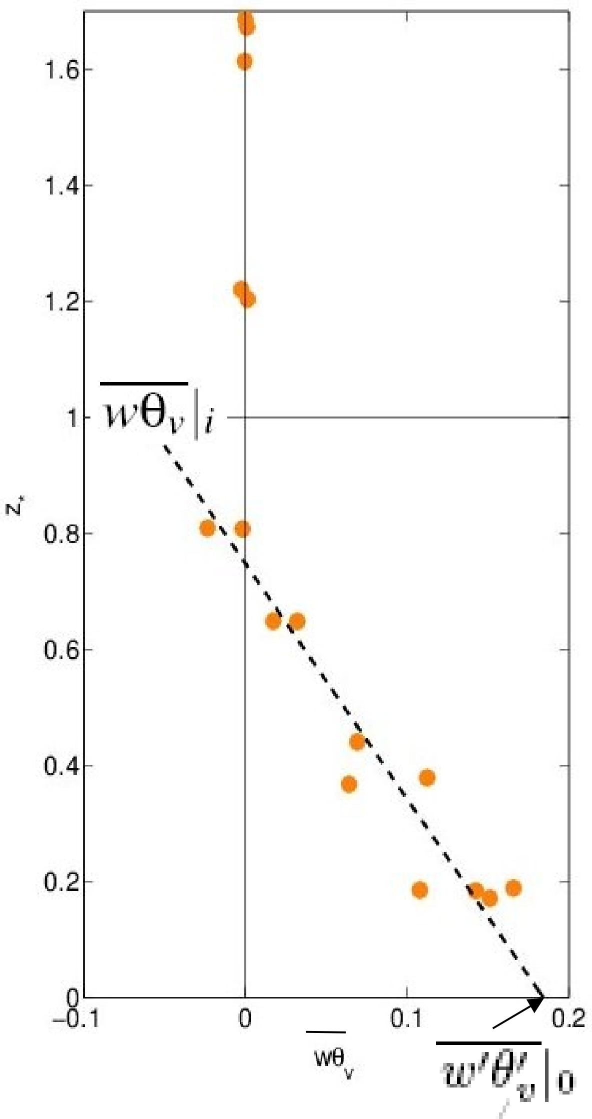

$$\beta = -\frac{\overline{w'\theta'_v}|_i}{\overline{w'\theta'_v}|_0}$$

$$w_e \simeq -\frac{\overline{w's'}|_i}{\Delta s}$$

Boundary layer growth and warming

$$\Delta\theta_v = \frac{\gamma\beta Z_i}{1+2\beta}$$

$$\frac{\partial\overline{\theta_v}}{\partial t} = -\frac{\partial\overline{w'\theta_v'}}{\partial z}$$

$$= \frac{\overline{w'\theta_v'}|_0 - \overline{w'\theta_v'}|_i}{Z_i}$$

$$w_e = (1+2\beta)\frac{\overline{w'\theta_v'}|_0}{\gamma Z_i}$$

Boundary layer scaling

- Deardoff velocity scale (Turbulent mixing during free convection)

$$w^* = \left[\frac{g z_i}{T_v} \overline{w' \theta'_s}\right]^{1/3} \sim 1 \tfrac{m}{s}$$

(z_i, θ'_s): Depth of the BL and potential temperature perturbation at surface.

- Friction velocity (Statically neutral conditions):

$$u^* = (\overline{u'w'}^2 + \overline{v'w'}^2)^{1/4}$$

- Obukhov length (Statically Noneutral conditions)

$$L = \left(\frac{-u^{*3}}{k\left(g/T_v\right)\left(\overline{w'\theta'}\right)_s}\right)$$

(k): Von Karman constant.

- Convective mixed layer time scale: $t^*_{ML} = \left(\frac{z_i}{w^*}\right)$

Flying strategies

defined as a function of (consensus between):

Scientific goals

and

Capability of the aircraft

(autonomy, minimum and maximum heights, airspeed, payload/instruments,…)

NCAR C130 during DYCOMS-II

(DYNAMICS AND CHEMISTRY OF MARINE STRATOCUMULUS)

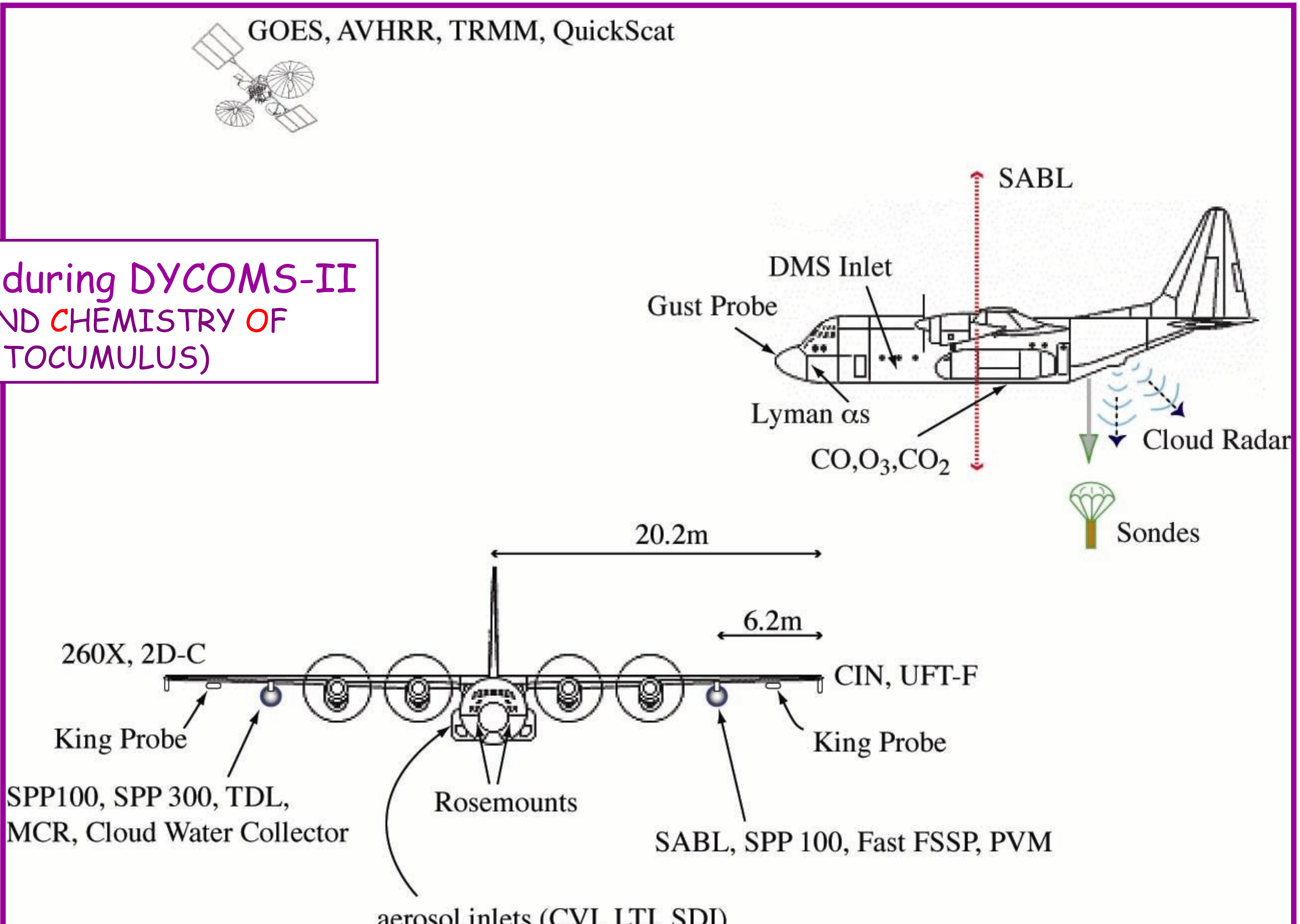

Stevens et al., *BAMS*, **84** (2003)

Studying the boundary layer vertical structure

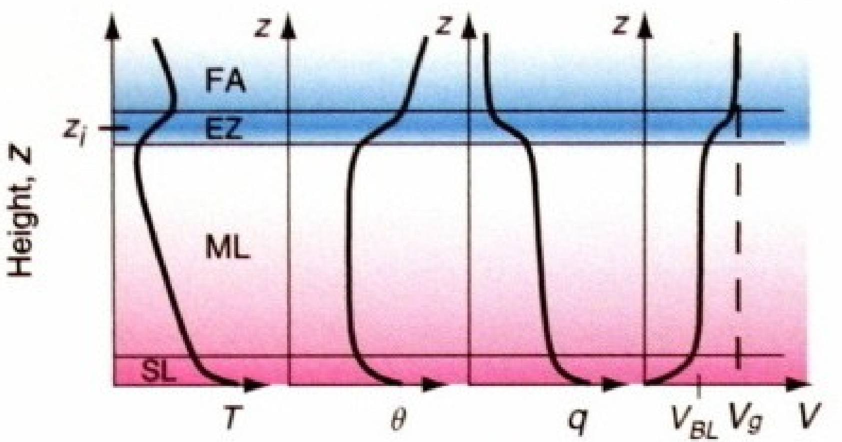

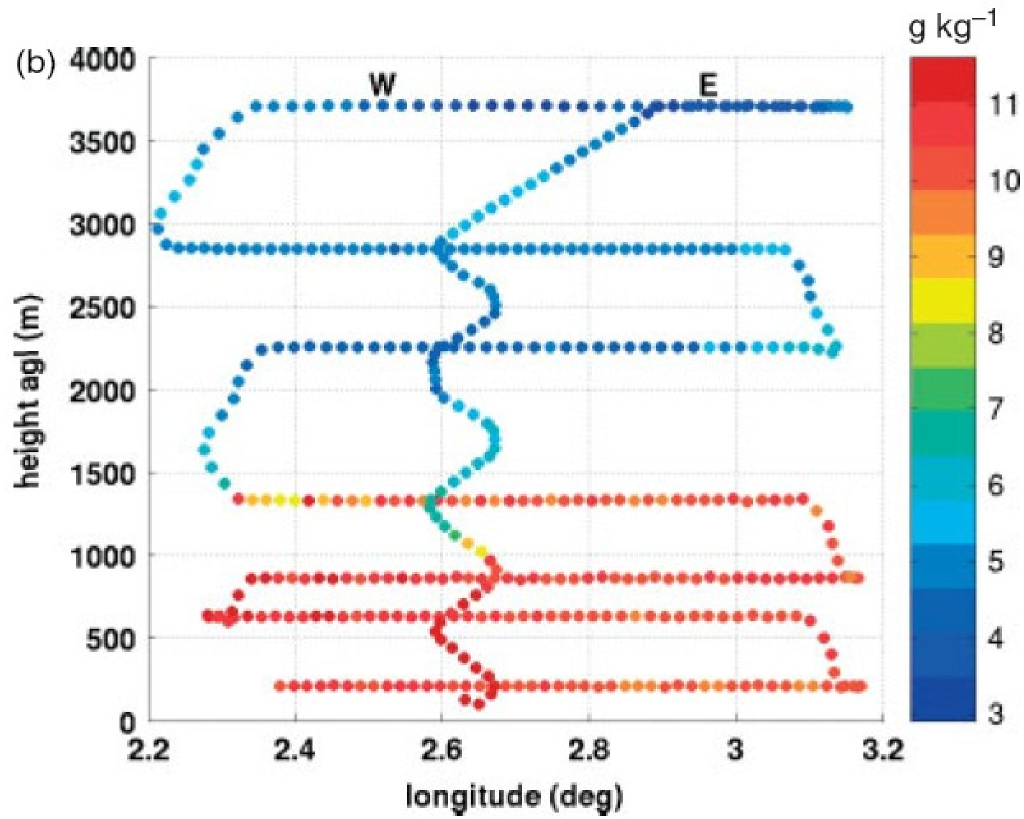

DYCOMS-II

DYNAMICS AND CHEMISTRY
OF MARINE
STRATOCUMULUS

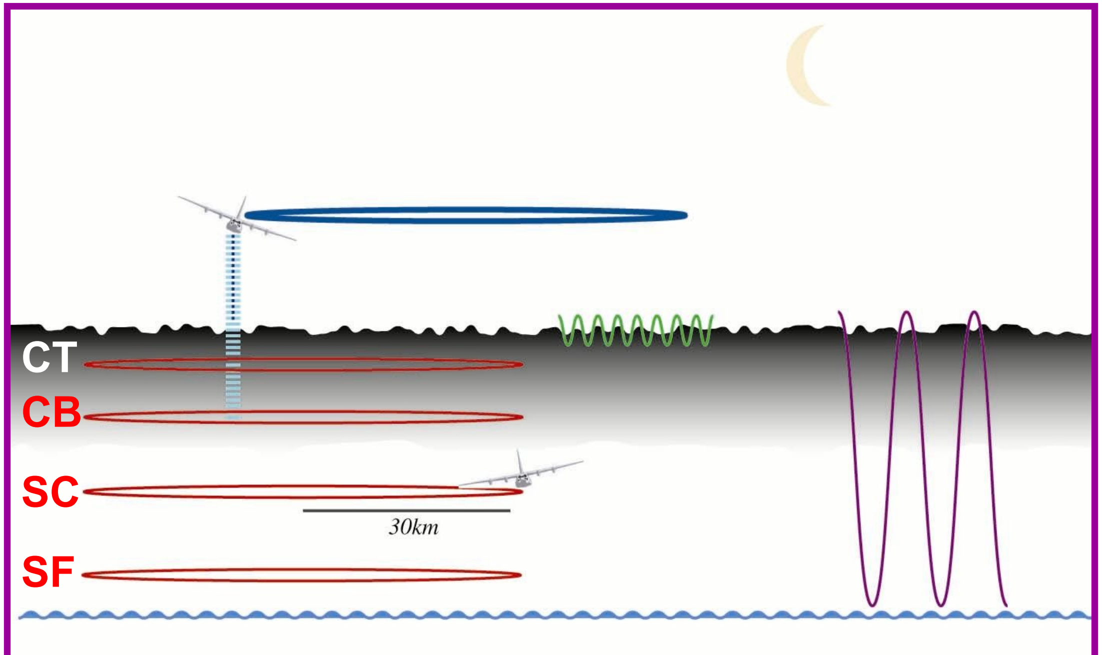

Stevens et al., *BAMS*, **84** (2003)

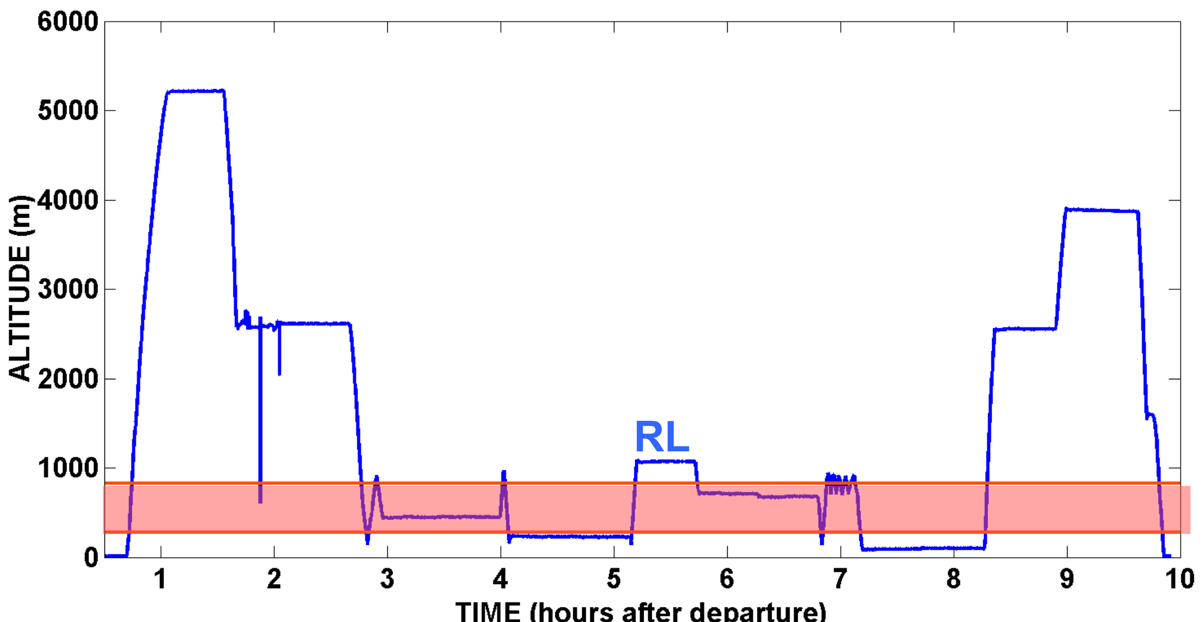

Fine-scale structure at stratocumulus cloud top

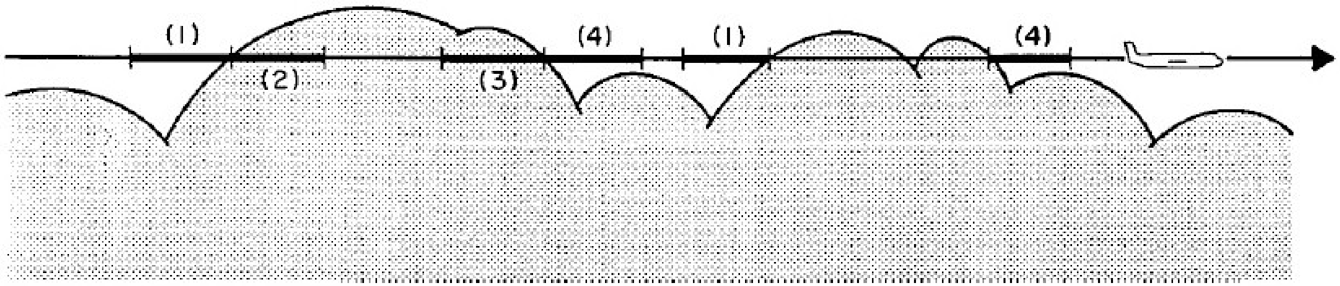

Figure 1. Schematic diagram showing the categories of segments referenced to cloud top that are used in the composited profiles.

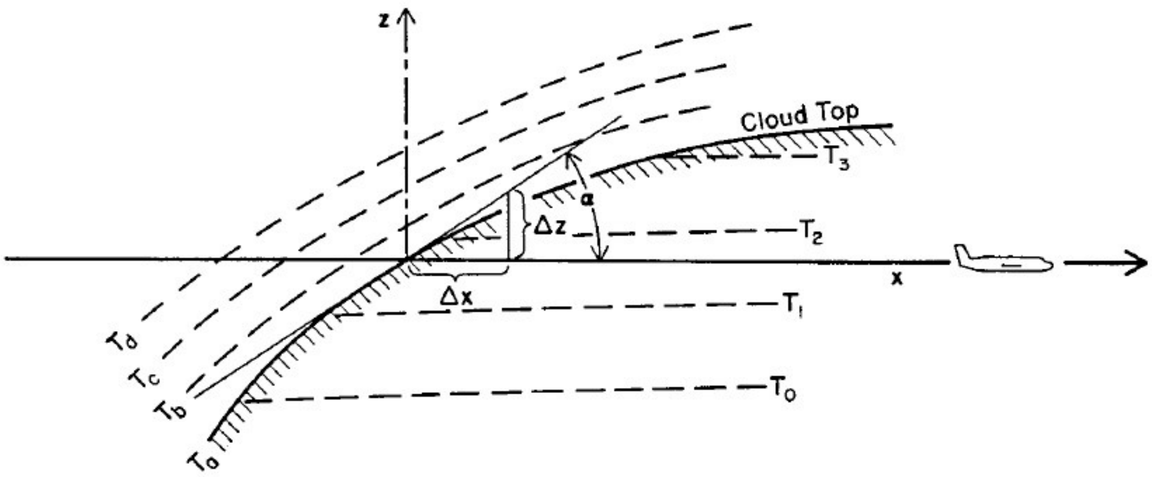

Figure 2. Schematic diagram showing the slope of the cloud at the airplane penetration point α and the assumed slopes of the isotherms above cloud-top (parallel to cloud-top) and inside the cloud (horizontal).

Lenschow et al, 2000

RICO

Rain In Cumulus over the Ocean

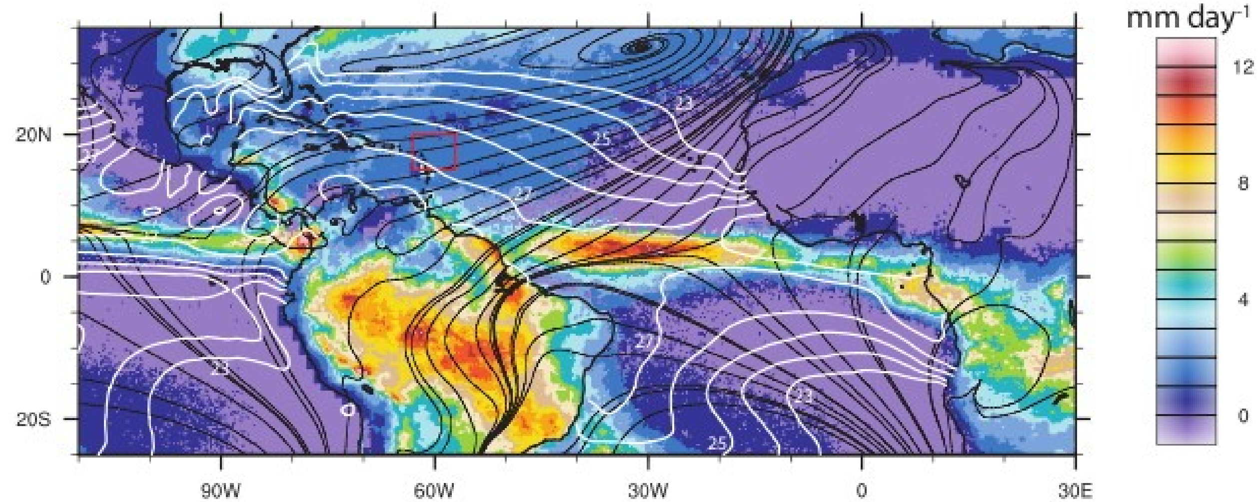

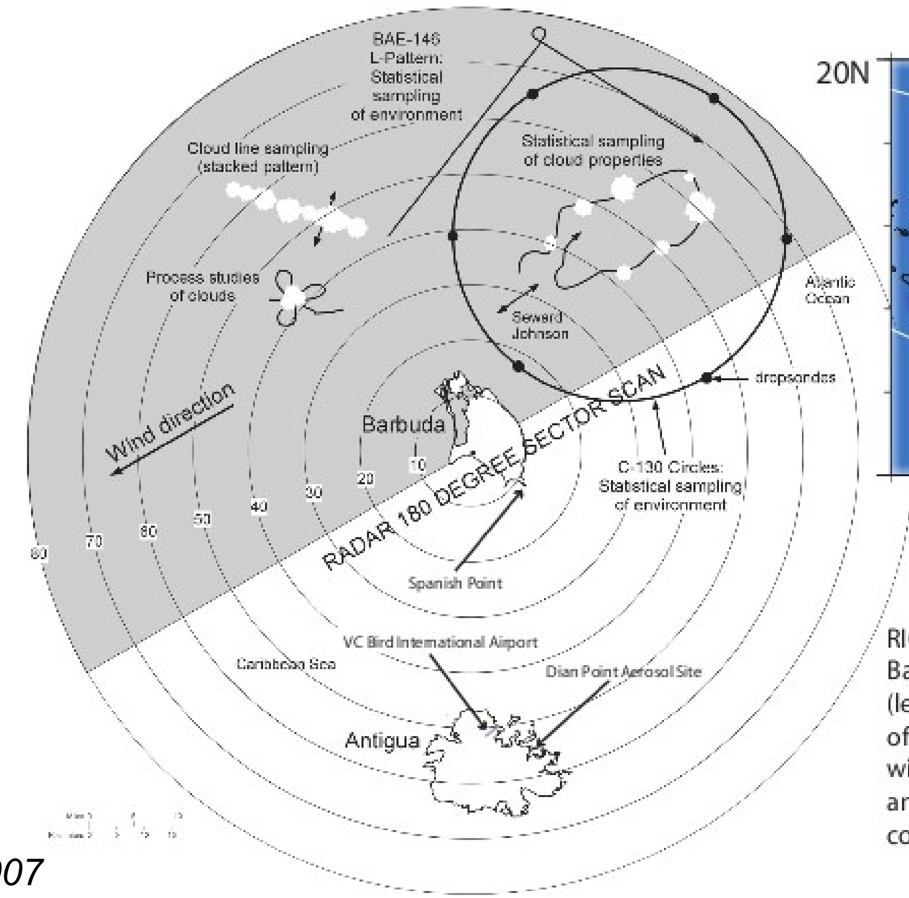

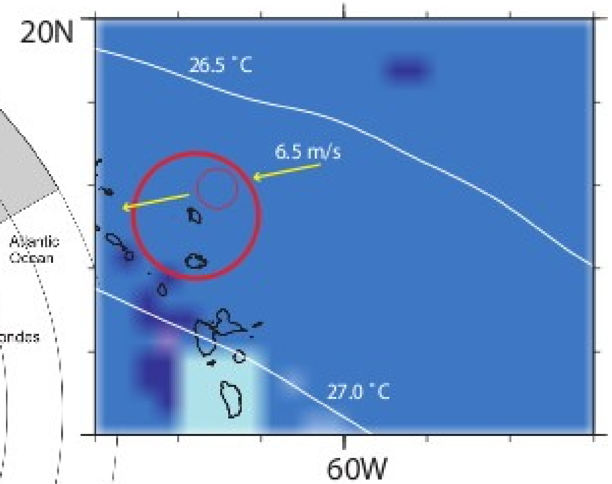

RICO observational domain at three scales: Basin (top), regional (above), operational (left). Color plots show Dec-Jan climatology of rainrates from TRMM contoured, 10m wind from ERA40 (black streamlines on top and yellow arrows above), and SSTs in white contours from Reynolds et al., (2002).

Rauber, Stevens et al, 2007

HiCu

High Plains Cumulus

Damiani and Vali, 2007

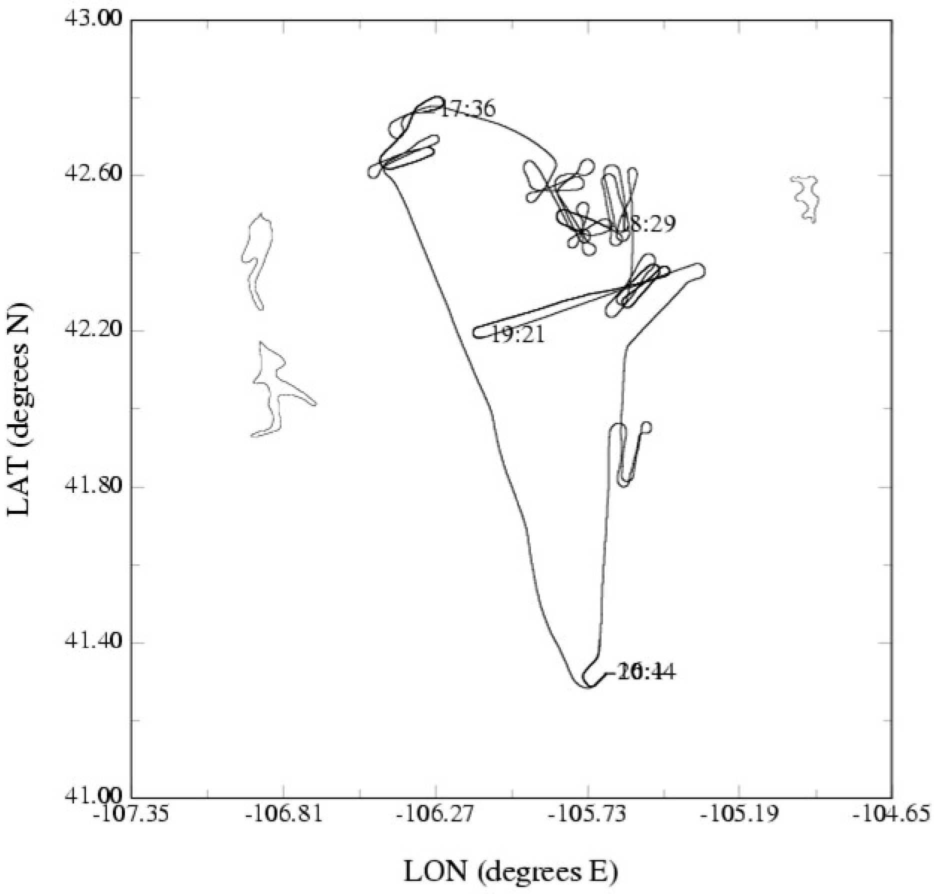

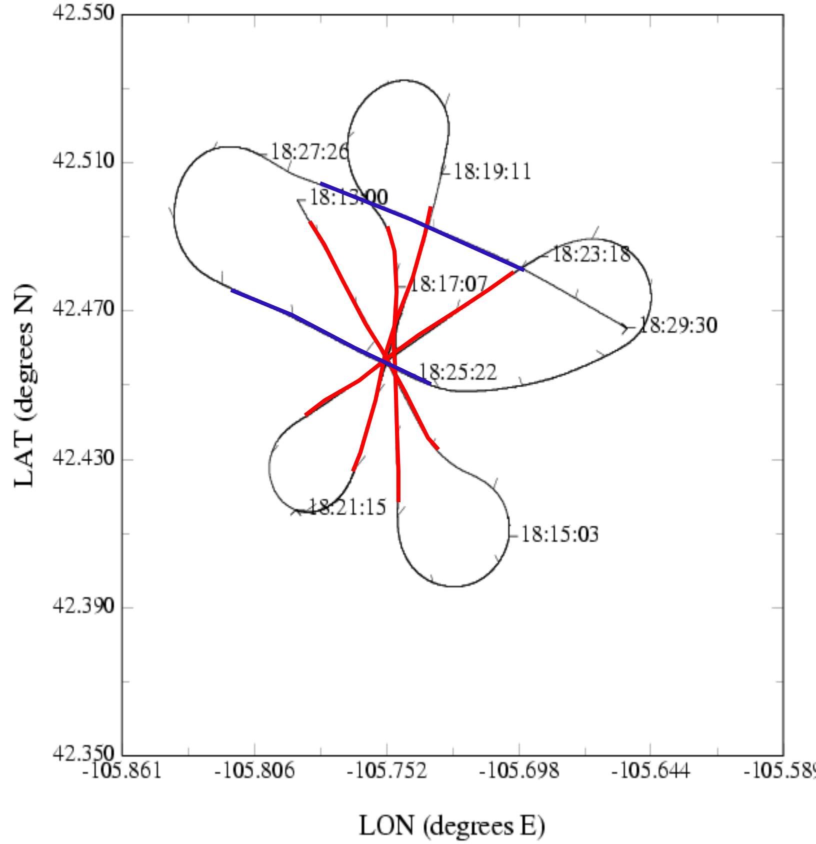

CuPIDO

Cumulus, Photogrammetric, In situ and Doppler Observations

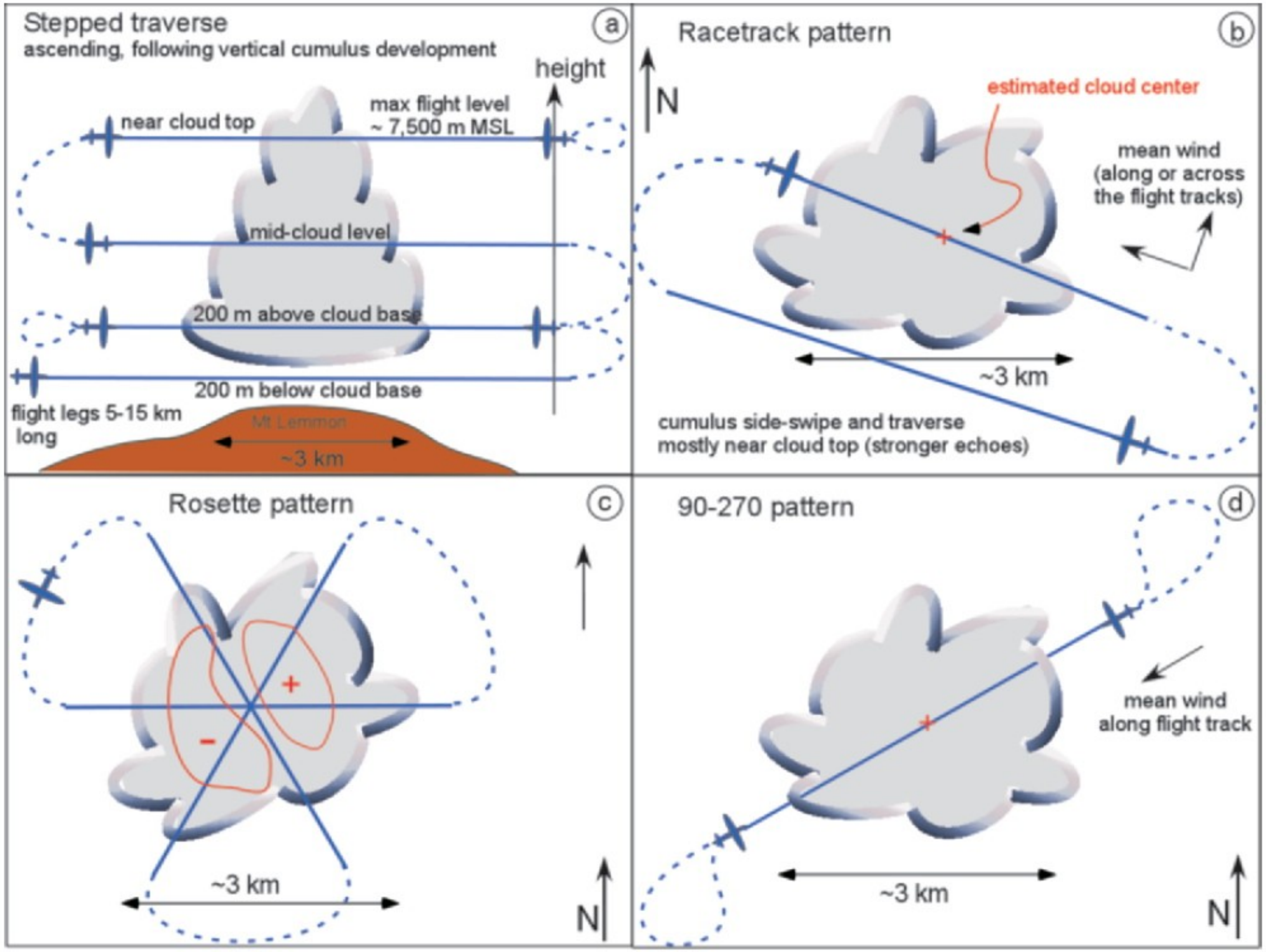

FIG. 3. Flight patterns used for cumulus dynamics studies.

Damiani et al, 2008

CuPIDO

Cumulus, Photogrammetric, In situ and Doppler Observations

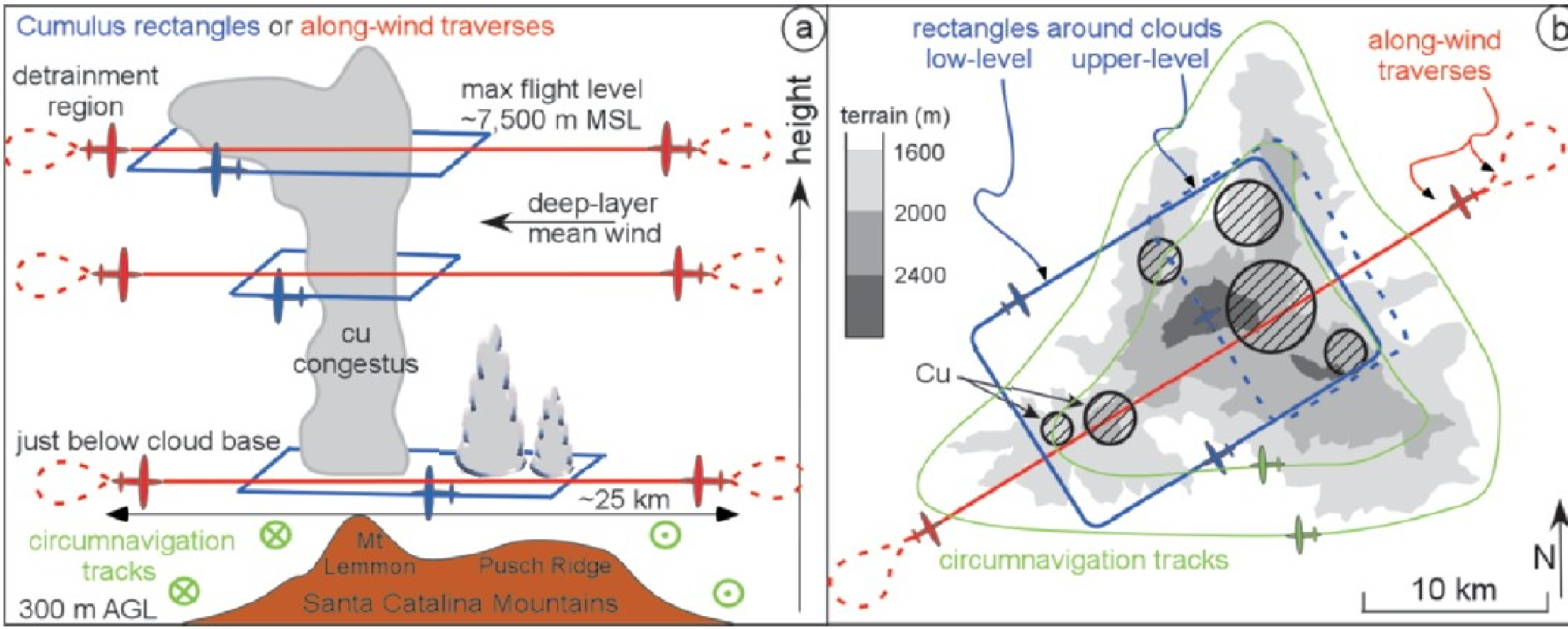

Fig. 4. Flight patterns used for BL dynamics and detrainment studies.

Damiani et al, 2008

95 GHz WYOMING CLOUD RADAR

Antennas diameter	**25 cm**
Peak power	**1.6 kW**
Pulse length	**250 ns (33 m)**

Beam width	**0.7°**
Repetition frequency	**5 kHz / 20 kHz**
Number of profiles per sec	**20 – 27**

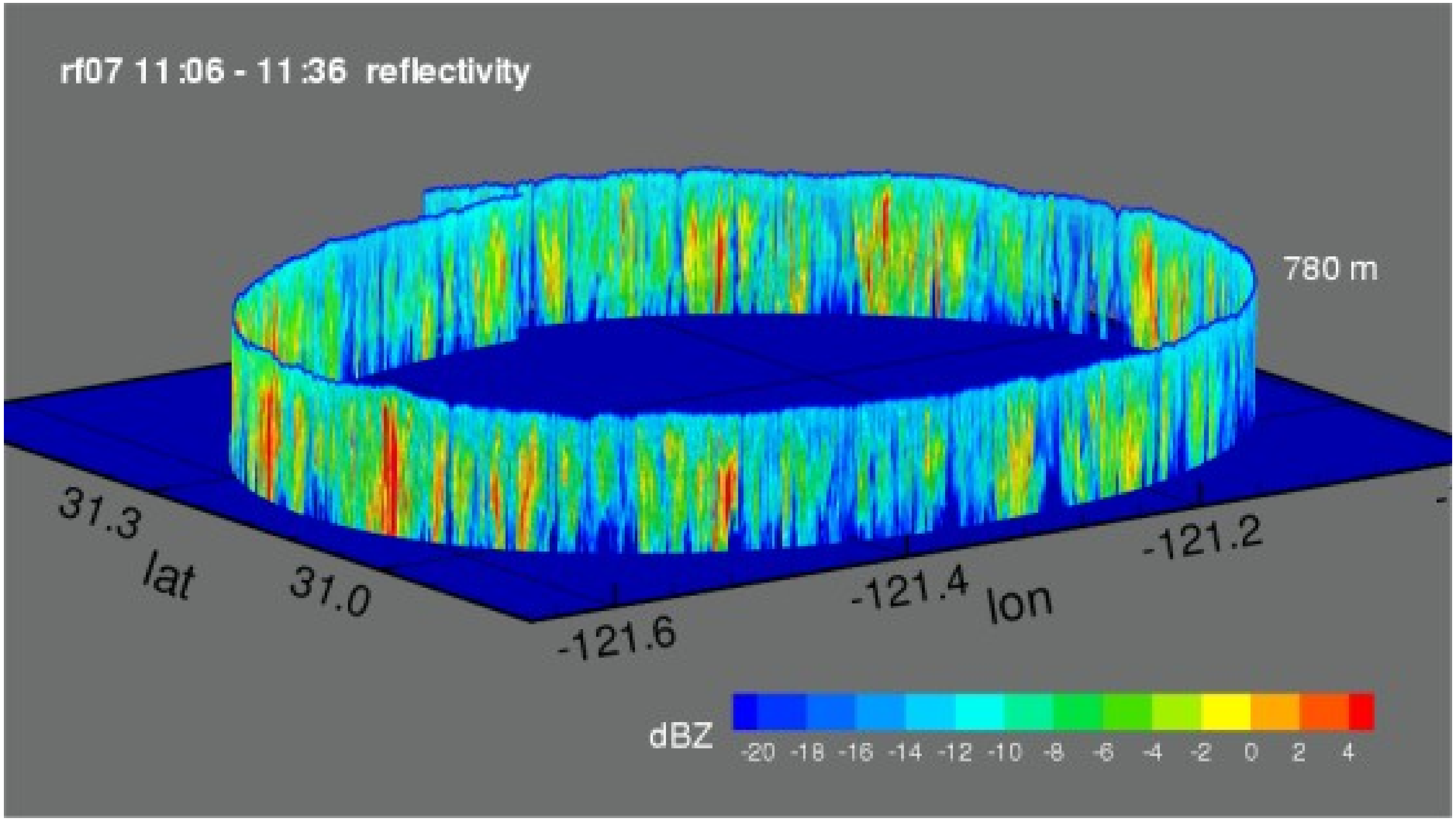

growing cell

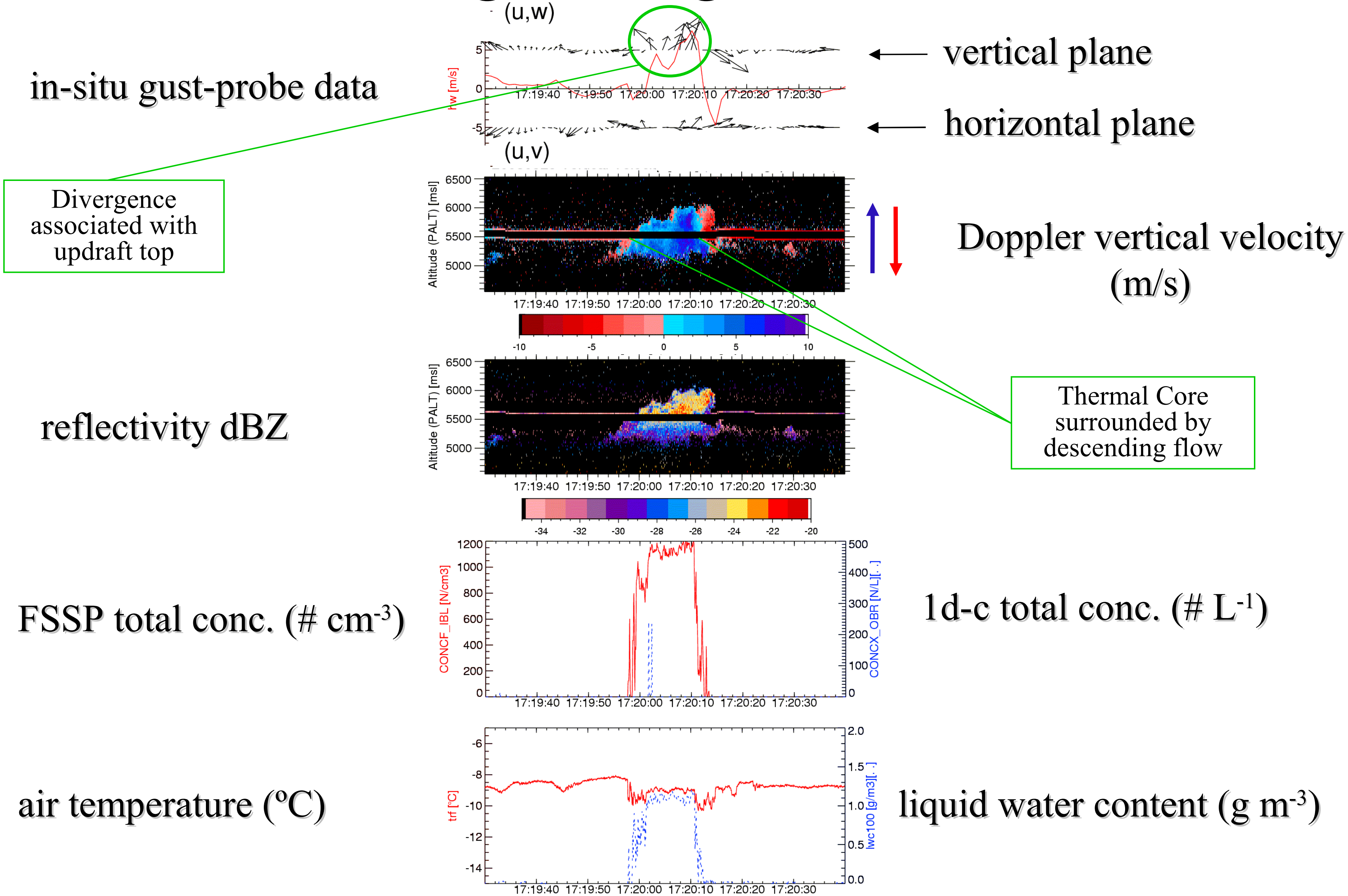

Aug 26th, 2003

thermal top 1st pass

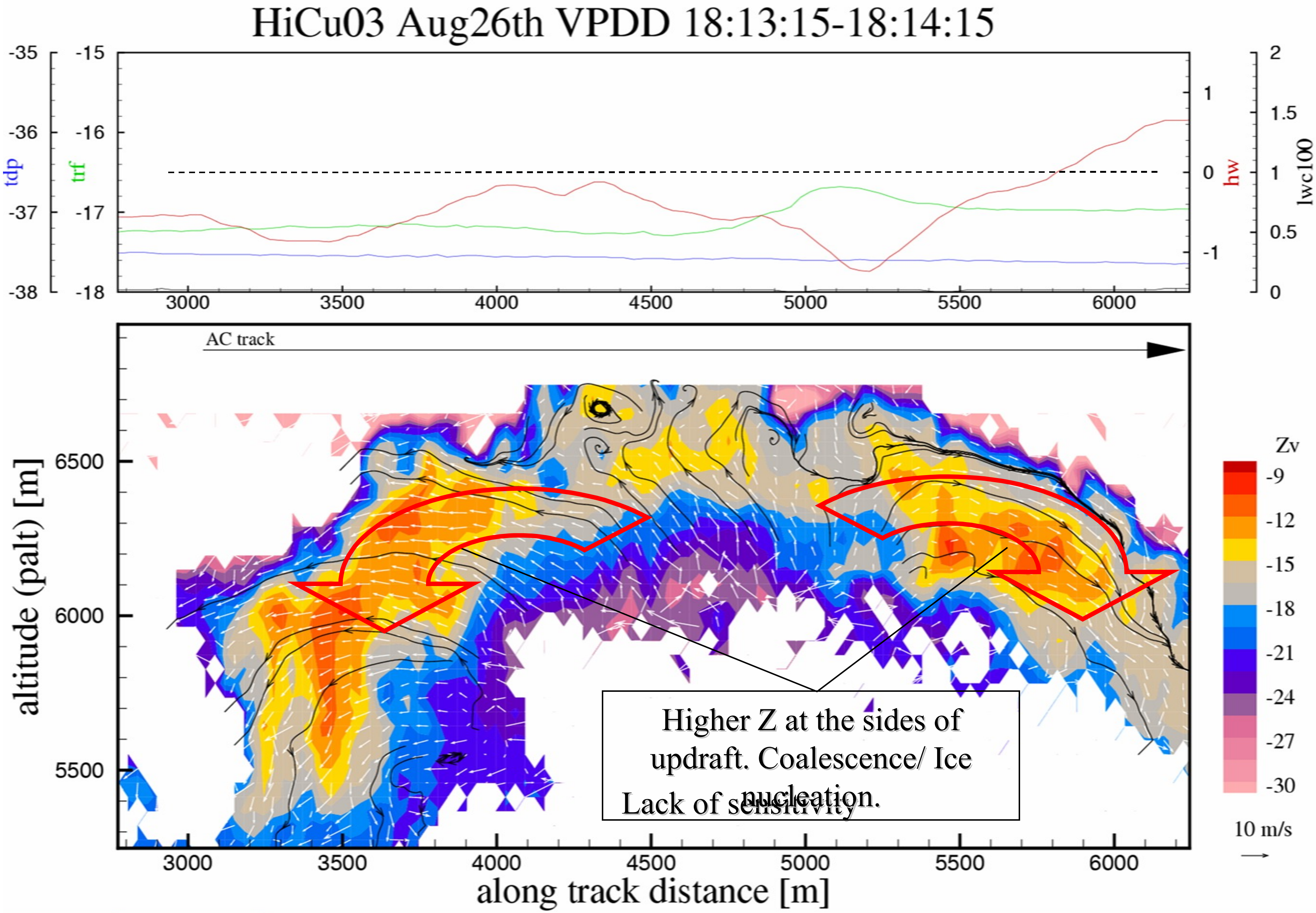

July 13th HBDD: final stages

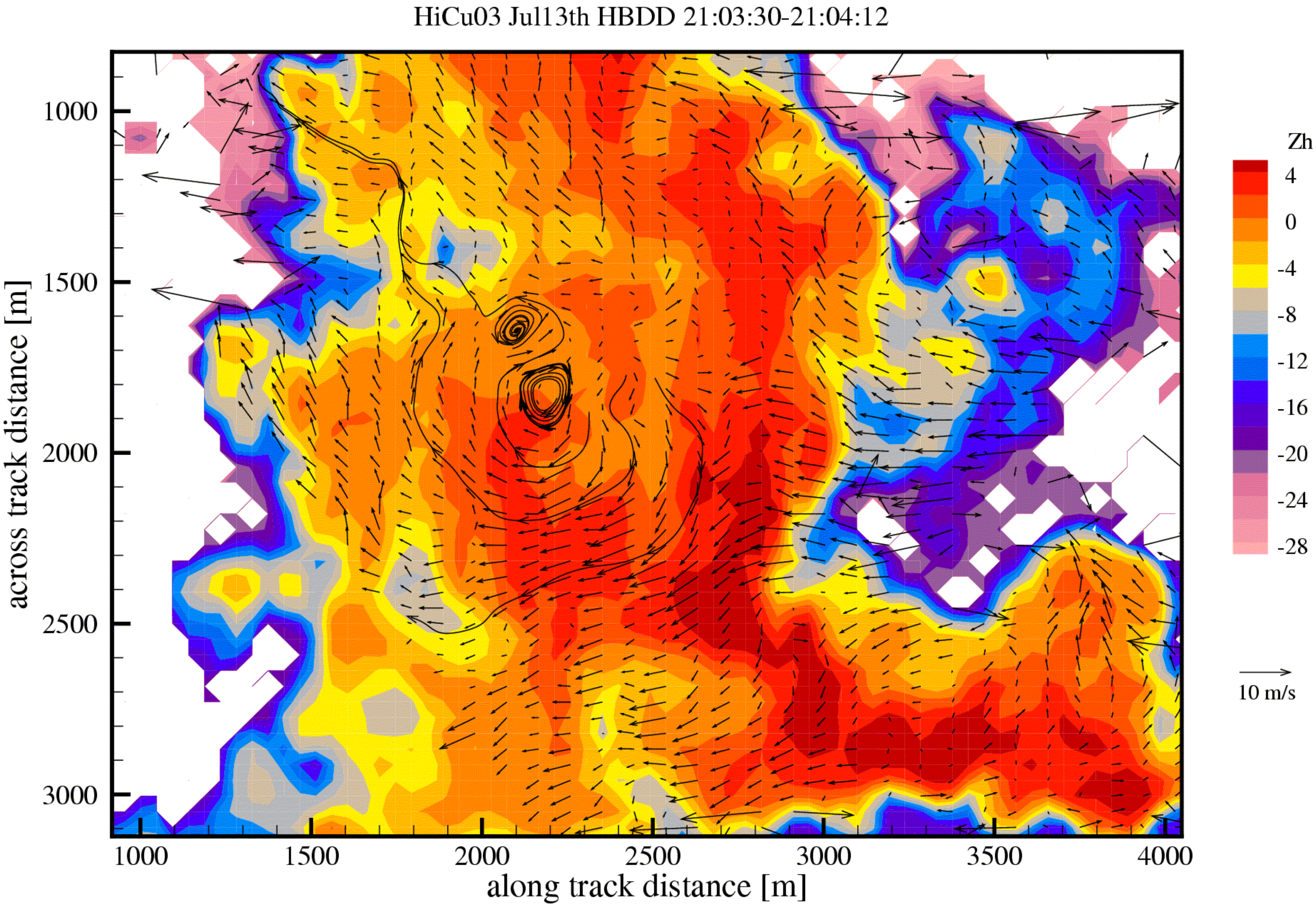

Jul 13th, 2003

Organized large scale horizontal dynamics

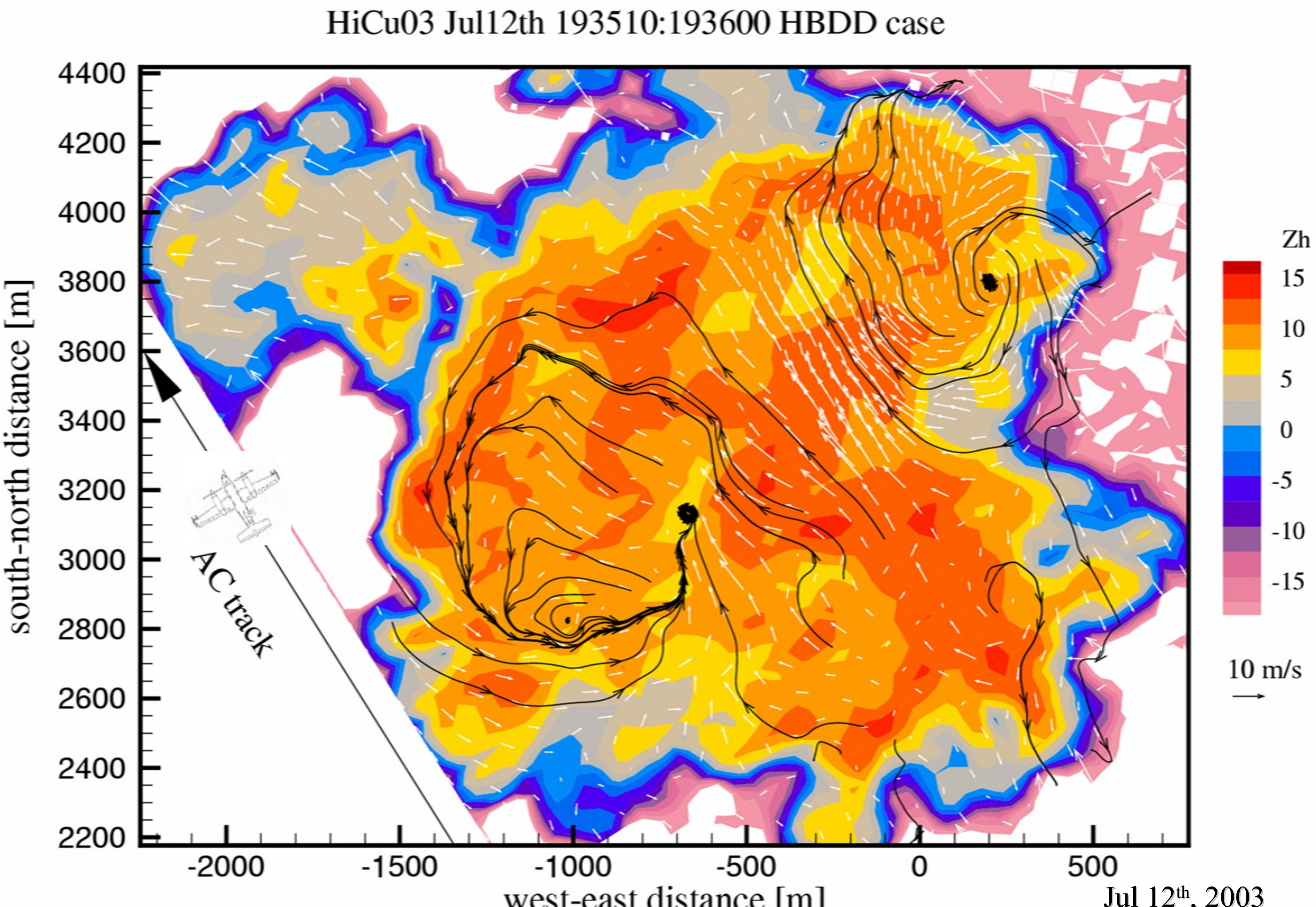

Jul 12th, 2003

References - Textbooks

Garratt, J. R. : The Atmospheric Boundary Layer. *Cambridge Atmospheric and Space Science Series, 1992, 316 pp.*

Lenschow, D. H. : Probing the Atmospheric Boundary Layer. *American Meteorological Society, Boston, Massachusetts, 1976, 269 pp.*

Monin, A. S. and A. M. Yaglom: Statistical Fluid Mechanics II. *Massachusetts Institute Technology Press , 1975, 874 pp.*

Stull, R. B. : An Introduction to the Atmospheric Boundary Layer Meteorology. *Kluwer Academin Publishers, 1988, 666 p.*

Wallace, J. M. and P. V. Hobbes: Atmospheric Science: An introductory Survey. *2d ed. Elsevier , 2006, 375-412.*

Wyngaard, J. C. : Turbulence in the Atmosphere. *Cambridge University Press, 2010, 393 pp.*

References - Articles

Canut, G., M. Lothon and F. Saïd, 2010: Observation of entrainment at the interface between monsoon flow and Saharan Air Layer, Quart. J. Roy. Meteorol. Soc., 136, 34-46.

Damiani R. and G. Vali, 2007: Evidence for tilted toroidal circulations in cumulus. J. Atmos. Sci., 64, 2045-2060.

Damiani, R., et al, 2008: The cumulus, photogrammetric, in situ, and Doppler observations experiment of 2006: Bull. Am. Met. Soc., 89, 57-+

Lemone, M. A., 1973: The structure and dynamics of horizontal vortices in the planetary boundary layer. J. Atmos. Sci., 30, 1077-1091.

Lenschow, D. H, J. Mann and L. Kristensen, 1994: How long is long enough when measuring fluxes and other turbulence statistics ? J. Atmos. Oceanic Technol.,
11, 661-673.

Lenschow, D. H. et al 2000: Measurements of the fine-scale structure at the top of Marine Stratocumulus. Boundary-Layer Meteorol., 97, 331-357.

Mann J. and D. H. and Lenschow, 1994: Errors in airborne flux measurements. J. Geophys. Res., 99, 14519-14526.

References - Articles

Stevens, B., 2005: Atmospheric Moist Convection. Annu. Earth Planet. Sci. 32, 605-643.

Stevens, B., 2006: Bulk boundary layer concepts for simplifed models of tropical dynamics, *heoretical and Computational Fluid Dyn.,* **20**, 279–304

Stevens, B. et al, 2007: On the structure of the lower troposphere in the summertime stratocumulus regime of the northeast Pacific, *Mon. Weath. Rev*, **135**, 985–1005.

Stevens B. et al 2003, Dynamics and Chemistry of Marine Stratocumulus - DYCOMS-II, Bull. Amer. Meteor. Soc., 84, 579-593.

Van Zanten, M. C. and B. Stevens, 2005: Observations of the structure of heavily precipitating marine stratocumuls, *J. Atmos. Sci.,* **62**, 4327–4342.

Weckwerth, T. M., 1997: Horizontal convective rolls: Determining the environmental conditions supporting their existence and characteristics. Mon. Wea. Rev., 125, 505-526.

Rauber, R. M., B. Stevens et al, 2007: Rain in (shallow) cumulus over the ocean—The RICO campaign, *Bull. of the American Meteorol. Soc.,* **88**, 1912–1928.